ISSN 2738-0971
eISSN 2738-1013

Bulletin of Natural Sciences Research

Vol. 11, Nº 2, 2021.

BULLETIN OF NATURAL SCIENCES RESEARCH

Published by
Faculty of Sciences and Mathematics, University of Priština in Kosovska Mitrovica
Republic of Serbia

Focus and Scope

Bulletin of Natural Sciences Research is an international, peer-reviewed, open access journal, published semiannually, both online and in print, by the Faculty of Sciences and Mathematics, University of Priština in Kosovska Mitrovica, Republic of Serbia. The Journal publishes articles on all aspects of research in biology, chemistry, geography, geoscience, astronomy, mathematics, computer science, mechanics and physics.

Technical Secretary

Danijel B. Đošić

Editorial Office

Ive Lole Ribara 29; 38220, Kosovska Mitrovica, Serbia, e-mail: editor@bulletinnsr.com, office@bulletinnsr.com; fax: +381 28 425 397

Printed by

Sigraf, Ćrila i Metodija bb, 37000 Kruševac, tel: +38137427704, e-mail: stamparijasigraf@gmail.com

Available Online

This journal is available online. Please visit http://www.bulletinnsr.com to search and download published articles.

BULLETIN OF NATURAL SCIENCES RESEARCH

Vol. 11, N^{o} 2, 2021.

CONTENTS

BIOLOGY

CHEMISTRY

PHYSICS

Bulletin of Natural Sciences Research
Vol. 11, No. 2, 2021, pp. 1-7.

DOI: https://doi.org/10.5937/bnsr11-25709
Original Scientific Paper

DIATOM SPECIES COMPOSITION AND THEIR SEASONAL DYNAMICS IN THE TIMOK RIVER BASIN

NIKOLA ĐUKIĆ[1,*], TATJANA JAKŠIĆ[1], OLIVERA PAPOVIĆ[1], PREDRAG VASIĆ[1]

[1]Faculty of Sciences and Mathematics, University of Priština in Kosovska Mitrovica, Kosovska Mitrovica, Serbia

ABSTRACT

The aim of this paper was to present the composition and seasonal dynamics of epilthic diatoms in the Timok River basin. The diatom samples were collected along the Timok River basin in March, May, August and November 2017. Permanent diatom slides were prepared after oxidizing the organic material by the hydrogen peroxide (H_2O_2). The cleaned diatom materials were mounted on permanent slides using ZRAX glue. A total of 85 taxa were identified in the Timok River Basin. The benthic diatom taxa belong to 31 genera with the highest diversity observed within *Navicula* Bory (15), *Nitzschia* Hassall (12) and *Gomphonema* Ehrenberg (8). Quantitative analysis showed that in all seasons, *Achnanthidium minutissimum* and *Amphora pediculus* were dominant taxa. In May, they were joined by the *Achnanthidium pyrenaicum, Gomphonema olivaceum* and *Ulnaria ulna*; in August by the *Cocconeis placentula, Denticula kuetzingii, Melosira varians, Navicula metareichardtiana, Nitzschia capitellata, N. fonticola* and *N. palea*; in November by the *D. kuetzingii, G. olivaceum, G. pumilum, N. metareichardtiana, N. veneta, Nitzschia capitellata* and *N. palea* and in March by *A. pyrenaicum, Diatoma moniliformis, G. olivaceum, N. palea* and *U. ulna*. Our research is the floristical and ecological study of benthic diatoms in this basin and can form the groundwork for further research work.

Keywords: Benthic diatoms, Species composition, Seasonal dynamics, Ecology, Timok River.

INTRODUCTION

Diatoms are a species rich group of eukaryotic unicellular microalgae and one of the most common organic matters in aquatic ecosystem (Wojtal, 2009). They play an important role the primary producers in freshwater and marine environments (Sarthou et al., 2005; Ishii et al., 2011). Diatoms are found in all aquatic habitats and in moist terrestrial habitats (Mann & Vanormelingen, 2013). They are cosmopolitan, with a wide geographical distribution and well-known autecology of most species (Wu et al, 2011; Van Dam et al., 1994). The taxonomic structure of diatom communities in rivers and streams is conditioned by water temperature, nutrient concentration, water flow, amount of light, grazing effect, substrate type and size (Wu et al., 2016). The impact of topography (altitude, longitude and latitude), geographically climatic characteristics (Tison et al., 2005), as well as glaciation (Stevenson et al., 1996), geomorphological characteristics and land use (Leland & Porter, 2000) must certainly not be neglected. The distribution, quality and quantity of diatom taxa on a temporal scale also depend on the characteristics of the species (growth rate, size) and the ecological niche of the species, since species of a broad ecological spectrum are more able to tolerate fluctuation of ecological factors in habitats than species with narrow ecological valences. The main study objectives were to present the floristic richness and seasonal dynamics of diatoms in the Timok River basin.

MATERIAL AND METHODS

The Timok is a across-border river. Most of the basin is located in eastern Serbia (98 %), while the smaller part is in the territory of Bulgaria (Paunović et al., 2008). It belongs to the Black Sea basin. The Timok River is formed by the joining of the Beli Timok and Crni Timok rivers downstream of the town Zaječar. The Beli Timok is formed by the joining of the Svrljiški Timok and Trgoviški Timok rivers on the northern outskirts of the town Knjaževac. Timok is the largest river of eastern Serbia, the right and last tributary of the Danube in Serbia, which flows into the Danube at 845.65 river km and not far from the mouth of the Timok river is the border of Serbia and Bulgaria. In the area of the Timok River basin, the so-called Timok river system is being developed for water supply for hydroelectric power plants, supply for settlements and water industry, irrigation, and tourist valorization of watercourses (Paunović et al., 2008).

Data on previous studies of diatoms in the Timok River basin are scarce. The first data on algological investigations date from 1996 and relate to the Trgoviški Timok River, when 143 taxa from 7 phyla were identified: *Cyanophyta* (24), *Rhodophyta* (3), *Xanthophyta* (2), *Chrysophyta* (1), *Bacillariophyta* (100), *Euglenophyta* (1) and *Chlorophyta* (12) (Simić, 1996). With regard to exploration of other rivers in the Basin, data are rare and relate to the diatoms of the tributaries of the Beli Timok (Ćirić et al., 2018) and the Crni Timok (Nikitović & Laušević, 1995), as well as other groups of *Chlorophyta* and *Rhodophyta* algae in the Svrljiški, Trgoviški and Beli Timok rivers (Simić et al., 2002; Simić & Ranković, 1998a, 1998b; Simić, 1995).

* Corresponding author: nikola.djukic@pr.ac.rs

The sampling was conducted during four seasons (March, May, August and November 2017) from 8 localities (Figure 1, Table 1) covering evenly the whole length of of the watercourse. Benthic diatoms were collected from a depth of 20-30 cm by brushing the stones with a toothbrush following Taylor et al. (2005). The samples were immediately fixed in 4% formaldehyde (HCHO).

Table 1. Characteristics of the 8 sampling stations along the Timok River basin.

No.	*River*	*Sampling site*	*Sampling site code*	*Latitude* (°)	*Longitude* (°)	*Altitude(m)*
1	Trgoviški Timok	Štrbac	ST5	43.50306	22.31861	359
2	Beli Timok	Drenovac	BT2	43.68944	22.26944	177
3	Zlotska reka	Zlot	CT4	44.00583	21.98466	261
4	Lubnička reka	Lubnica	CT7	43.8585	22.19266	225
5	Crni Timok	Zvezdan	CT8	43.89166	22.22166	147
6	Borska reka	Kriveljska_Reka	BR5	44.03333	22.21667	231
7	Borska reka	Rgotina	BR7	44.00688	22.26733	153
8	Timok	Vražogrnac	VT1	43.9555	22.32017	111

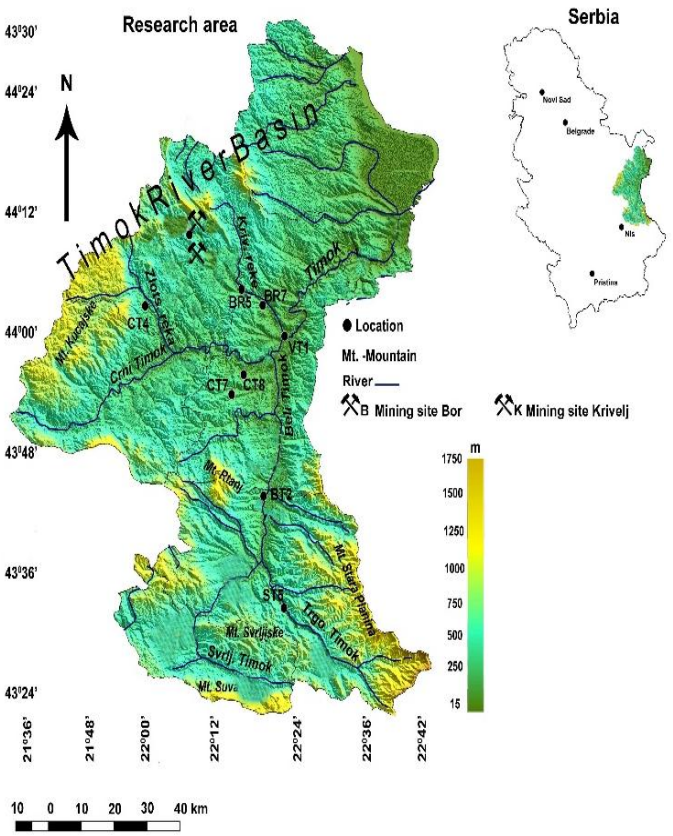

Figure 1. The Timok River basin and sampling stations.

At each site pH, conductivity, temperature and salinity were measured using a multiparameter device (PCSTester 35K), which was calibrated beforehand.

Diatom frustules were cleaned using 10% cold hydrochloric acid (HCL) and 30% hydrogen peroxide (H_2O_2) to remove organic matter from the sample according to the standard method described by Taylor et al. (2005). All samples were washed several times with distilled water, then the material was mounted in ZRAX glue and permanent slides were made. The relative abundance (%) of the identified taxa was determined by counting 400 valves on each slide on the same microscope that used for qualitative analysis of diatoms, and at 1000 x magnification (EN 14407, 2014).

Diatom species were identified according to Lange Bertalot et al. (2017) and Levkov (2009).

In order to analyse the diversity of epilithic diatom assemblages at different sampling sites and in different seasons, Shannon's Diversity Index was computed along with Pielou's evenness index following the calculations described in Heip et al. (1998).

RESULTS AND DISCUSION

Values of the physical and chemical water characteristics from 8 sampling sites are presented in Table 2 and Table 3. The water temperature during the sampling period varied from 5.4°C (CT7) in March to 23.2°C (VT1) in August. pH ranged from 5 (BR7) in March to 8.8 (VT1) in August. Electrical conductivity values varied from 232 µS cm-1 (ST5) to 4310 µS cm-1 (BR7) and salinity from 0,1‰ (ST4) to 2,32‰ (BR7).

A total of 85 taxa were identified in the Timok River basin. The benthic diatom taxa of the Timok River basin belong to 31 genera with the highest diversity observed in *Navicula* (15), *Nitzschia* (12) and *Gomphonema* (8). The largest number of taxa was identified at the CT8 site (44) in May and August; in November, all localities are distinguished by a similar number of taxa (27 -35) and in March, the largest number of taxa was identified at the BR7 and VT1 sites (both 37 each). The smallest number of taxa was present at the sampling site CT7 (18) in May; in August at sampling site BR5 (17) and in March at the sampling site ST5 (18). *Achnanthidium minutissimum* (Kützing) Czarnecki, *Achnanthidium pyrenaicum* (Hustedt) Kobayasi, *Amphora pediculus* (Kützing) Grunow, *Cocconeis placentula* Ehrenberg, *Diatoma moniliformis* (Kützing) D. M. Williams, *Gomhonema olivaceum* (Hornemann) Brébisson, *Gomphonema pumilum* (Grunow) E. Reichardt & Lange-Bertalot, *Navicula cryptonella* Lange-Bertalot, *Navicula metareichardtiana* Lange-

Bertalot & Kusber, *Navicula tripunctata* (Müller) Bory de Saint-Vincent, *Nitzchia dissipata* (Kützing) Rabenhorst, *Nitzschia fonticola* (Grunow) Grunow, and *Nitzschia palea* (Kütz.) W. Smith were the most frequent taxa in the Timok basin, represented in over 75% of the samples. The same taxa are also dominant.

Table 2. Values of the physical and chemical water characteristics from 8 sampling sites of the Timok River basin in March and May.

Season and site	March 2017								May 2017							
Parameter	ST5	BT2	CT4	CT7	VT1	BR5	BR7	CT8	ST5	BT2	CT4	CT7	VT1	BR5	BR7	CT8
Temperature (°C)	6,3	7,3	7,3	5,4	8,3	8,6	7,8	7,5	10,8	13,7	12,5	12,3	14,7	15,8	15,2	13,5
pH	8,2	8,2	8,2	8,5	8,6	5,3	5,0	8,2	8,4	8,3	8,4	8,4	8,3	6,7	5,4	8,4
Conductivity (µS/cm)	232,0	411,0	280,0	685,0	438,0	1168,0	1433,0	401,0	258,0	436,0	322,0	710,0	466,0	1630,0	1896,0	421,0
Salinity (‰)	0,1	0,2	0,1	0,3	0,2	0,6	0,7	0,2	0,1	0,2	0,2	0,3	0,2	0,8	1,0	0,2

Table 3. Values of the physical and chemical water characteristics from 8 sampling sites of the Timok River basin in August and November.

Season and site	August 2017								November 2017							
Parameter	ST5	BT2	CT4	CT7	VT1	BR5	BR7	CT8	ST5	BT2	CT4	CT7	VT1	BR5	BR7	CT8
Temperature (°C)	17,2	21,4	20,3	16,0	23,2	19,7	21,5	22,7	6,6	8,0	9,8	8,0	8,8	8,9	8,9	7,8
pH	8,4	8,5	8,5	8,4	8,8	6,3	6,0	8,5	8,2	8,2	8,4	8,0	8,7	6,5	5,3	8,3
Conductivity (µS/cm)	338,0	530,0	433,0	1290,0	564,0	3000,0	4310,0	464,0	232,0	402,0	409,0	887,0	502,0	1865,0	1753,0	537,0
Salinity (‰)	0,2	0,3	0,2	0,6	0,3	1,6	2,3	0,2	0,1	0,2	0,2	0,4	0,2	0,9	0,8	0,2

Halamphora montana (Krasske) Levkov, *Pantocsekiella ocellata* (Pantocsek) K. T. Kiss & Ács, *Cymbella neolanceolata* W. Silva, *Odontidium mesodon* (Kützing) Kützing, *Diploneis oculata* (Brébisson) Cleve, *Eunotia pectinalis f. undulata* (J. Ralfs) Berg, *Fallacia subhamulata* (Grunow) D. G. Mann, *Gyrosigma acuminatum* (Kützing) Rabenhorst, *Karayevia ploenensis* (Hustedt) Bukhtiyarova, *Navicula amphiceropsis* Lange-Bertalot & Rumrich, *Navicula reichardtii* Grunow, *Navicula viridulacalcis* Lange-Bertalot, *Nitzschia linearis var. tenuis* (Smith) Gr. in Cleve & Gr., *Nitzschia vermicularis* (Kützing) Hantzsch in Rabenhorst, *Pinnularia obscuriformis* Krammer and *Tryblionella apiculata* W. Gregory were present at only one locality. Quantitative analysis showed that in all seasons, *A. minutissimum* and *A. pediculus* were present with a percentage with 10% or more at least at one locality (Table 4, Table 5). In May, they were joined by the *A. pyrenaicum*, *G. olivaceum* and *Ulnaria ulna* (Nitzsch) Compère; in August by the *C. placentula*, *Denticula kuetzingii* Grunow, *Melosira varians* C. Agardh, *N. metareichardtiana*, *Nitzschia capitellata* Hustedt in Schmidt et al., *N. fonticola* and *N. palea*; in November by *the D. kuetzingii, G. olivaceum, G. pumilum, N. metareichardtiana*, *Navicula veneta* Kützing, *N. capitellata* and *N. palea* and in March by *A. pyrenaicum, D. moniliformis, G. olivaceum, N. palea and U. ulna*.

The Timok River basin is dominated by taxa that often occur in samples, as well as a large number of taxa that occur sporadically, which is typical of many rivers (Szabóet et al., 2005; Chatháin & Harrington, 2008; Makovinska & Hlubikova, 2015). *A. minutissimum* and *A. pediculus* were dominant taxa in all four seasons. These taxa are cosmopolitan and have widespread distribution in the epilithic communities of diatoms of many rivers (Potapova & Charles, 2003; Bere & Tundisi, 2011). *A. minutissimum* is a widespread taxon in acidic, base, oligo- to hypereutrophic waters (Van Dam et al., 1994; Wojtal & Sobczyk, 2006). *A. pediculus* is a widespread freshwater species that occasionally inhabits eutrophic and moderately polluted waters (Levkov, 2009). It is an alkalophilic species, which often occurs in waters with moderate conductivity (Van Dam et al., 1994), and is absent from acidic habitats with low electrolyte concentration (Lange-Bertalot et al., 2017). The most abundant genera were:*Navicula*, *Gomphonema*a nd *Nitzschia*. This is to be expected, since researches in Serbia (Andrejić et al., 2012; Vidaković et al., 2015; Jakovljević et al., 2016a, 2016b; Vasiljević et al., 2017) and other countries (Hlúbiková et al., 2009; Sevindik & Kucuk, 2016; Noga et al., 2016) have shown that these three genera are dominant in the epilithic community.

Changes in the physical and chemical characteristics of water over time affect the seasonal dynamics of the diatom communities. Taxon distribution from upper to lower parts of the stream, water ionic composition and pH and temperature values are the three most important environmental factors that affect the structure of diatom communities on a temporal and spatial scale (Potapova & Charles, 2002). Diatoms are known to respond to annual variations in water temperature (Di Pippo et al., 2012; Lambert et al., 2016). *C. placentula* may increase abundance in the summer months, as observed in studies by Ní Chatháin & Harrington (2008) who found a greater number of this taxon during the early summer, while the *Gomphonema olivaceum* is adapted to lower temperatures (Potapova & Charles, 2002), which is consistent with our findings (seen in Table 4 and Table 5). Also, Wojtal & Sobczyk (2006) point out that appearance of certain taxa with higher relative representation may be related to the seasonal shift of diatom communities. They found an increased abundance of species of the genus *Navicula* in November, while the research by Ní Chatháin & Harrington (2008) showed that the species of the genus *Gomphonema* are

more common in the autumn, which is consistent with our results indicating an increased relative representation of species of genus *Navicula* (*N. metareichardtiana* and *N. veneta*) and species of genus *Gomphonema* (*G. pumilum*) during the said period. *G. pumilum* is considered to be the most widespread species of the genus *Gomphonema*, occurring in rivers and streams with limestone bedrock, inhabits oligosaprobic to β-mesosaprobic water and can be tolerant of medium to high trophic level pollution (Lange-Bertalot et al., 2017). Undernatural conditions, water temperature and its annual variation depend on other factors (DeNicola, 1996).

Table 4. Diatom taxa with a percentage with 10% or more at least at one locality in the Timok River basin in 2017, in March and May.

Season and site	March 2017								May 2017							
Taxa	ST5	BT2	CT4	CT7	VT1	BR5	BR7	CT8	ST5	BT2	CT4	CT7	VT1	BR5	BR7	CT8
Achnanthidiumpyrenaicum	73,9	0,5	1,7	0,0	0,0	7,7	2,9	7,4	38,0	0,4	44,8	0,0	1,5	9,5	1,4	2,4
Achnanthidiumminutissimum	0,0	1,4	45,2	1,4	4,8	44,5	33,5	13,4	3,0	8,9	32,9	6,3	6,1	34,2	53,0	8,7
Amphora pediculus	4,8	20,5	1,9	12,7	2,5	0,0	1,3	12,4	18,8	49,1	6,2	74,6	61,3	2,0	0,4	7,2
Diatoma moniliformis	0,0	0,2	2,6	0,0	10,7	0,0	2,7	2,5	1,9	1,8	0,2	0,5	0,0	3,2	1,9	7,5
Gomphonema olivaceum	5,0	54,7	3,8	35,6	22,0	0,0	4,1	18,8	3,2	8,9	2,9	6,8	2,9	0,0	0,5	18,6
Ulnaria ulna	0,0	0,0	0,0	2,6	10,7	2,5	1,0	2,5	1,4	2,2	0,0	0,5	1,5	0,5	2,9	11,3

Table 5. Diatom taxa with a percentage with 10% or more at least at one locality in the Timok River basin in 2017, in August and November.

Season and site	August 2017								November 2017							
Taxa	ST5	BT2	CT4	CT7	VT1	BR5	BR7	CT8	ST5	BT2	CT4	CT7	VT1	BR5	BR7	CT8
Achnanthidium Minutissimum	1,4	3,5	45,7	2,7	3,7	71,5	58,0	2,3	1,9	10,2	39,5	0,5	1,7	26,5	29,3	5,4
Amphora Pediculus	8,6	18,1	2,6	35,3	5,2	0,7	2,6	64,8	21,4	13,8	22,6	5,1	7,7	5,0	0,7	48,4
Cocconeis Placentula	52,2	45,3	0,0	0,0	1,2	0,5	0,9	2,7	5,6	2,2	0,5	1,5	1,2	1,5	1,9	1,3
Denticula Kuetzingii	0,5	1,7	0,0	42,0	0,5	0,0	1,9	0,0	0,9	12,1	0,0	0,0	1,0	0,5	3,7	0,0
Gomphonema Olivaceum	3,5	5,2	4,5	1,4	4,0	3,5	0,8	3,9	21,4	13,6	1,4	0,5	3,7	0,5	1,5	6,7
Gomphonema Pumilum	7,2	1,7	3,3	3,4	2,2	0,5	0,9	3,4	21,1	19,1	2,1	1,9	2,5	1,5	0,9	5,8
Melosira Varians	0,0	0,0	11,5	0,5	0,0	2,5	3,8	0,5	0,2	0,0	1,6	0,0	0,2	0,0	4,2	0,0
Navicula metareichardtiana	0,7	0,0	2,9	0,5	11,9	0,5	1,4	0,7	1,2	3,9	0,5	0,5	12,9	3,0	0,5	4,0
Navicula Veneta	0,0	0,0	0,0	0,0	0,0	0,0	0,0	0,0	0,0	0,0	0,0	3,9	21,6	1,5	0,0	0,0
Nitzschia Capitellata	1,6	0,0	0,5	0,5	10,7	0,0	0,0	0,2	0,0	0,0	0,9	26,5	8,2	2,0	0,8	0,9
Nitzschia Fonticola	0,5	0,7	6,2	0,5	20,4	0,0	1,4	0,2	0,5	1,7	5,1	2,4	0,7	4,0	0,0	1,8
Nitzschia palea	0,0	1,4	4,5	0,0	22,6	0,0	4,7	0,9	0,5	3,9	2,3	26,2	24,1	9,5	7,6	0,9

As mentioned, the lower species richness of diatom assemblage was identified at BR5, which also had the acid reaction of water and highest values of conductivity (seen in Table 2 and Table 3). This was expected due to the mining-industrial complex Bor located after the BR5. Also, Verb & Vis (2000) reported that the species richness are typically reduced at acid mine drainage (AMD) site. The highest values of the Shannon's Diversity Index (Shannon &Weaver, 1949) at almost all localities along the Timok River basin were recorded in November while the lowest were during the summer (Figure 2). In November, the values of the diversity index at almost all localities were above 3, and it was observed that the diversity of codominant taxa in the community increased and their distribution was the most uniform. The Pielou's evenness index (Pielou, 1966) follow the upward trend, ie. decreases in the value of the diversity index per season (Figure 3). Research of diatoms of the Velika Morava in Serbia has also shown the highest number of diatom taxa in the autumn (Vasiljević, 2017). The diversity index, as well as the structure of dominant taxa,

suggests a very similar community along the Timok River Basin with noticeable seasonal changes.

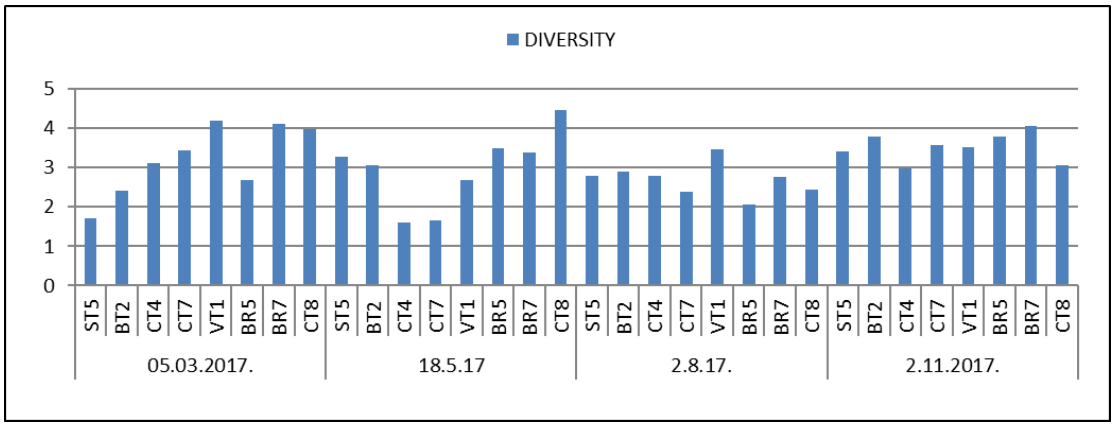

Figure 2. Shannon-Wiener Diversity Index during four seasons at the sampling sites (Figure 2) on the Timok Basin.

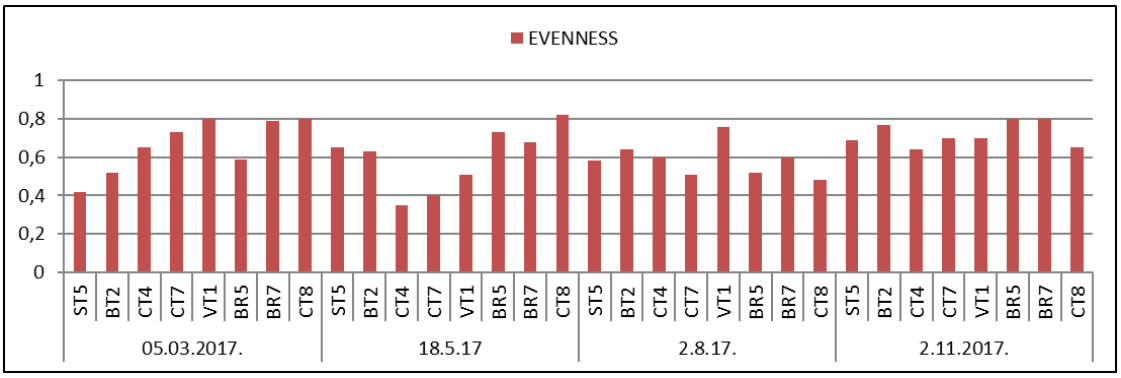

Figure 3. Pielou's evenness index during four seasons at the sampling sites (Figure 3) on the Timok Basin.

CONCLUSION

In this study, it was aimed to explore the composition and seasonal abundance of diatoms in the Timok River basin.

In terms of benthic diatom communities, previous data from the Timok River Basin is scattered. The presented data increase our knowledge of the river system, which is important for further prediction of diatoms as bioindicators; however, further fundamental investigations are necessary since the diatom microflora in this part of the Balkan Peninsula have been insufficiently studied regardless of a relatively long period of research.

REFERENCES

Andrejić, Z. J., Krizmanić, J. & Cvijan, M. 2012. Diatom species composition of the Nišava river and its tributaries Jerma and Temska rivers (Southern Serbia), Arch. Biol. Sci., 64(3), pp. 1127-1140. doi.org/10.2298/ABS1203127A

Bere, T. & Tundisi, J. G. 2011. Diatom-based water quality assessment in streams influence by urban pollution: effects of natural and two selected artificial substrates, São Carlos-SP, Brazil, Braz. J. Aquat. Sci. Technol, 15(1), pp. 54-63.

Chatháin, N. B. & Harrington, J. T. 2008. Benthic diatoms of the River Deel: Diversity and Community Structure,Biology & Environment-proceedings of the Royal Irish Academy, 10, pp. 29-42. doi:10.3318/BIOE.2008.108.1.29

DeNicola, D. M. 1996. Periphyton responses to temperature at different ecological levels. In: Stevenson, R. J., Bothwell, M. L. Lowe, R. L. (eds.). Algal Ecology: Freshwater Benthic Ecosystems. San Diego: Academic, pp. 150-176.

Di Pippo, F., Ellwood N. T. W., Guzzon, A., Siliato L., Micheletti, E., De Philippis, R. & Albertano P. B. 2012. Effect of light and temperature on biomass, photosynthesis and capsular polysaccharides in cultured phototrophic biofilms, J. Appl. Phycol., 24(2), pp. 211-220. doi: 10.1007/s10811-011-9669-0

EN 14407, 2014. Water quality. Guidance for the identification and enumeration of benthic diatom samples from rivers and lakes. Geneva: Comité European de Normalisation.

Heip, C. H. R., Herman, P. M. J. & Soetaert, K. 1998. Indices of diversity and evenness, Oceanis, 24(4), pp. 61-87.

Hlúbiková, D., Blanco, S., Falasco, E., Gomà, J., Hoffmann, L. & Ector, L. 2009. *Nitzschia alicae*sp. nov. and *N. puriformis*sp. nov., new diatoms from European rivers and comparison with the type material of *N. sublinearis* and *N. pura*, Journal of Phycology, 45(3), pp. 742-760. doi.org/10.1111/j.1529-8817.2009.00692.x

Ishii, K. I., Iwataki, M., Matsuoka, K. & Imai, I. 2011. Proposal of identification criteria for resting spores of *Chaetoceros* species (Bacillariophyceae) from a temperate coastal Sea, Phycologia, 50, pp. 351-362. doi.org/10.2216/10-36.1

Jakovljević, O., Popović, S., Živić, I., Stojanović, K. & Krizmanić, J. 2016a. Benthic diatoms of the Vrla River (Serbia) and their application in the water ecological status assessment, Oceanological and Hydrobiological Studies, 45(3), pp. 304-315. doi: 10.1515/ohs-2016-0029

Jakovljević, O., Popović, S., Vidaković, D., Stojanović, K. & Krizmanić, J. 2016b. The application of benthic diatoms in water quality assessment (Mlava River, Serbia), Acta Botanica Croatica, 75(2), pp. 199-205. doi.org/10.1515/botcro-2016-0032

Lambert, A. S., Dabrin, A., Morin, S., Gahou, J., Foulquier, A., Coquery, M. & Pesce, S. 2016. Temperature modulates phototrophic periphyton response to chronic copper exposure. Environ. Pollut., 208, pp. 821-829. doi:10.1016/j.envpol.2015.11.004

Lange-Bertalot, H., Hofmann, G., Werum, M. & Cantonati, M. 2017. Freshwater Benthic Diatoms of Central Europe: Over 800 Common Species Used in Ecological Assessment. Koeltz Botanical Books, 942 pp.

Leland, H. V. & Porter, S. D. 2000. Distribution of benthic algae in the upper Illinois River basin in relation to geology and land use, Freshwater Biology, 44(2), pp. 279-301. doi.org/10.1046/j.1365-2427.2000.00536.x

Levkov, Z. 2009. Amphora sensu lato. In: Lange-Bertalot, H. (Ed.), Diatoms of Europe: Diatoms of the European Inland Waters and Comparable Habitats vol. 5.A.R.G. Gantner Verlag K.G, 916 pp.

Makovinska, J. & Hlubikova, D. 2015. Phytobenthos of the River Danube. In: Liska, I. (ed.). The Handbook of Environmental Chemistry. The Danube River Basinvol. 39. Springer, Berlin, Heidelberg, pp. 317-340.

Mann, D. G. & Vanormelingen, P. 2013. An inordinate fondness? The number, distributions, and origins of diatom species, The Journal of Eukaryot Microbiology, 60(4), pp. 414-420. doi: 10.1111/jeu.12047

Nikitović, J. & Laušević, R. 1995. Algološka i saprobiološka analiza reke Beljevine (Jugoslavija), Ekologija, 30(1-2), pp. 27-39.

Noga, T., Stanek-Tarkowska, J., Kloc, U., Kochman-Kędziora, N., Rybak, M., Peszek, Ł. & Pajączek, A. 2016. Diatom diversity and water quality of a suburban stream: a case study of the Rzeszów city in SE Poland, Biodiv. Res. Conserv., 41, pp. 19-34. doi.org/10.1515/biorc-2016-0004

Paunović, M., Vassilev, V., Cheshmedijev, S. & Simić, V. 2008. Procena stanja životne sredine i rizika na slivu reke Timok. Rec Grey paper, pp. 58.

Pielou, E. C. 1966. The measurement of diversity in different types of biological collections, Journal of theoretical biology, 13, pp. 131-144. doi.org/10.1016/0022-5193(66)90013-0

Potapova, M. G. & Charles, D. F. 2002. Benthic diatoms in USA rivers: distributions along spatial and environmental gradients,Journal of Biogeography, 29(2), pp. 167-187. doi.org/10.1046/j.1365-2699.2002.00668.x

Potapova, M. & Charles, D. F. 2003. Distribution of benthic diatoms in US rivers in relation to conductivity and ioniccomposition, Freshwater Biology, 48(8), pp. 1311-1328. doi:10.1046/j.1365-2427.2003.01080.x

Sarthou, G., Timmermans, K. R., Blain, S. & Tréguer, P. 2005. Growth physiology and fate of diatoms in the ocean: a review, Journal of Sea Research, 53(1-2), pp. 25-42. doi.org/10.1016/j.seares.2004.01.007

Sevindik, T. O. & Kucuk, F. 2016. Benthic Diatoms as Indicators of Water Quality in the Acarlar Floodplain Forest (Northern Turkey), Fresenius Environmental Bulletin, 25(10), pp. 4013-4025.

Shannon, C. E. & Weaver, W. 1949. The Mathematical Theory of Communication. Urbana:University of Illinois Press.

Simić S. 1995. Bentosne zajednice algi Trgoviškog Timoka. Magistarska teza, Biološki fakultet, Univerzitet u Beogradu

Simić, S. 1996. The algae of Trgoviški Timok (Serbia, Yugoslavia). Bulletin of the Institute of Botany and Botanical Gardens, University of Belgrade, 30, pp. 107-118.

Simić, S. & Ranković, B. (1998a). New data on the distribution, morphology and ecology of red algae (Rhodophyta) in therivers of Serbia, Archives of Biological Sciences, 50(1), pp. 43-50.

Simić, S. & Ranković, B. (1998b). Contribution to the knowledge of bioindicator properties of red algae (Rhodophyta) in the Rivers of Serbia. 27th Conf. on Current Problems of Water Protection “Water Protection '98”, Kotor, Proc., pp. 399-404.

Simić, S., Cvijan, M. & Ranković, B. 2002. Distribution and ecology of green algae (Chlorophyta) in the watershead of the Timok river (Serbia), Ekologija, 37(1-2), pp. 23-32.

Szabó, K., Kiss, K. T., Taba, G. & Ács, É. 2005. Epiphytic diatoms of the Tisza River, Kisköre Reservoir and some oxbows of the Tisza River after the cyanide and heavy metal pollution in 2000, Acta Botanica Croatica, 64(1), pp. 1-46.

Stevenson, R. J., Bothwell, M. L., & Lowe, R. L. 1996. Algal ecology: Freshwater benthic ecosystem. San Diego: Academic press, CA, 753 pp.

Taylor, J. C., de la Rey, P. A. & van Rensburg, L. 2005. Reommendations for the collection, preparation and enumeration of diatoms from riverine habitats for water quality monitoring in South Africa, African journal of Aquatic Science, 30(1), pp. 65-75. doi.org/10.2989/16085910509503836

Tison, J., Park Y. S., Coste, M., Wasson, J. G., Ector, L., Rimet, F. & Delmas, F. 2005. Typology of diatom communities and the influence of hydro-ecoregions: A study on the French hydrosystem scale, Water Research, 39(14), pp. 3177-3188. doi.org/10.1016/j.watres.2005.05.029

Van Dam, H., Mertens, A. & Sinkeldam, J. 1994. A coded checklist and ecological indicator values of freshwater diatoms from the Netherlands, Aquatic Ecology, 28(1), pp. 117-133. doi.org/10.1007/BF02334251

Vasiljević, B., Simić, B. S., Paunović, M., Zuliani, T., Krizmanić, J., Marković, V. & Tomović, J. 2017. Contribution to the improvement of diatom-based assessments of the ecological status of large rivers – The Sava River Case Study, Science of the Total Environment, 605- 606, pp. 874-883.

Vasiljević, B. 2017. Bentosne silikatne alge (Bacillariophyta) u proceni ekološkog statusa reka Velike Morave i Save. Doktorska disertacija, Prirodno-matematički fakultet, Univerzitet u Kragujevcu, Kragujevac, pp. 142.

Verb, R. G. & Vis, M. L. 2000. Comparison of benthic diatom assemblages from streams draining abandoned and reclaimed coal mines and non-impacted sites, J. N. Am. Benthol.Soc., 19, pp. 274-288. doi:10.2307/1468070

Vidaković, D., Krizmanić, J., Šovran, S., Stojanović, K. & Đorđević, J. 2015. Diatom species composition in the Raška river (southwestern Serbia), Matica Srpska J. Nat. Sci., 128, pp. 29-40. doi:10.2298/ZMSPN1528029V

Wojtal, A. & Sobczyk, L. 2006. Composition and structure of epilithic diatom assemblages on stones of different size in a small calcareous stream (S Poland), Algological Studies, 119(1), pp. 105-124. doi: 10.1127/1864-1318/2006/0119-0105

Wojtal, A. 2009. Diatom flora of the Kobylanka stream near Kraków (Wyżyna Krakowsko-Częstochowska Upland, S Poland), Polish Botanical Journal, 54(2), pp. 129-330.

Wu, N. C., Schmalz, B. & Fohrer, N. 2011. A comparison of phytoplankton assemblages generated by two sampling protocols in a lowland catchment, Germany, Annales de Limnologie/International Journal of Limnology, 47, pp. 313-323. doi.org/10.1051/limn/2011045

Wu, N., Faber, C., Sun, X., Qu, Y., Wang, C., Ivetic, S., Riis, T., Ulrich, U.&Fohrer, N. 2016. Importance of sampling frequency when collecting diatoms, Scientific Reports, 6(36950), pp. 1-9.doi.org/10.1038/srep36950

Ćirić, M., Nikolić, N., Krizmanić, J., Gavrilović, B., Pantelić, A. & Petrović, V. 2018. Diatom diversity and ecological status of the Lasovačka and Lenovačka streams near Zaječar: Consideration of WFD implementation in Serbia, Archives of Biological Sciences, 70 (4), pp. 691-698. doi.org/10.2298/ABS180412032C

Bulletin of Natural Sciences Research
Vol.11, No.2, 2021, pp. 8-12.

DOI: https://doi.org/10.5937/bnsr11-29876
Original Scientific Paper

NEW DATA ON THE DISTRIBUTION OF LEPIDOPTERA IN MONTENEGRO, WITH A REVIEW OF ABERRANT FORMS

PREDRAG JAKŠIĆ[1] ⋆, **ANDREW KING**[2]

[1]Faculty of Sciences and Mathematics, University of Priština in Kosovska Mitrovica, Kosovska Mitrovica, Serbia
[2]Grovewood Close 18, Chorleywood, Hertfordshire, WD3 5PU, United Kingdom

ABSTRACT

During the three-year period of investigations, species from the families Depressariidae Meyrick, 1883, Pyralidae Latreille, 1809, Crambidae Latreille, 1810, Lycaenidae Leach, 1815, Nymphalidae Rafinesque, 1815, Geometridae Leach, 1815 and Erebidae Leach, 1815 were investigated. Investigations were carried out in 20 localities, distributed throughout the entire territory of Montenegro. Two species are listed for Montenegro for the first time: *Hypoxystis pluviaria* (Fabricius, 1787) and *Aspitates ochrearia* (Rossi, 1794).

Keywords: Lepidoptera, Montenegro.

INTRODUCTION

The moth fauna of Montenegro is still insufficiently surveyed. Only the area of NP "Durmitor" is well studied, thanks to the results of project "Fauna Durmitora", which was realized in the period 1980 – 1996. Montenegro deserves special attention due to its rich biodiversity. In two biogeographical regions (Mediterranean, and Alpine) representatives of different fauna (Tertiary relicts, glacial relicts and modern elements) are present. With the publication of such data, the knowledge about the Lepidoptera fauna of Montenegro would be significantly increased.

In the period 2017 – 2020, field work was performed with the aim of recording key species of Lepidoptera for the needs of the project of implementation of Natura 2000 in Montenegro. On that occasion, in addition to the species from Anex II of Habitat Directive 92/43, other species of Lepidoptera were also sampled. We present part of the determined results in this paper.

MATERIAL AND METHODS

This survey was carried out at 20 localities, distributed throughout the entire territory of Montenegro (Table 1). Butterflies were collected in a classical way, using entomological nets. The moths were collected using "Philips" Mercury Vapour Standard HPL lamps and pyramidal light traps, which used white neon lights and UV neon lights, supported by "Ultracell" UL7-12 (12V 7AH/20HR) batteries. The photos were taken with a Nikon D 3200 camera. Taxonomic order and nomenclature uses the scheme according to Nieukerken (2011) and Wiemers (2018).

RESULTS AND DISCUSSION

Results for 22 species from seven families are shown. Among them, several species deserve special attention:
Family Depressariidae Meyrick, 1883

Ethmia chrysopygella (Kolenati, 1846), Grlja waterfall, 992 m, 5 May 2017., two males. [Name according to: Domingo et al. (2003)]
Famyli Pyralidae Latreille, 1809

Selagia spadicella (Hübner, 1796), Durmitor Mt., Žabljak, Meždo, 1376 m, 21 July 2017., one male. Genitalia checked, slide CG-2892.

Pempeliella ornatella ([Denis & Schiffermüller], 1775), Montenegro, Durmitor, Žabljak, 1450 m, 5 June 2017., one male. Genitalia checked, slide CG-2915. *Eurhodope rosella* (Scopoli, 1763), Durmitor Mt., Žabljak, 1376 m,21 July 2017, one male.
Family Crambidae Latreille, 1810

Crambus hamella (Thunberg, 1788), Durmitor Mt., Žabljak, 1450 m, 5 June 2017, one male.

Figure 1. *Eurrhypis pollinalis* ([Denis & Schiffermüller], 1775).

Eurrhypis pollinalis ([Denis & Schiffermüller], 1775), Podgorica, Ćemovsko polje, 76 m, 2 June 2017., one male; Durmitor Mt., Goveđe jezero Lake, 1520 m, 6 June 2017, two males and

⋆ Corresponding author: jaksicpredrag@gmail.com

Table 1. List of the visited localities in Montenegro, by chronological order.

LOCALITY and DATE	ELEVATION (m a.s.l.)	COORDINATES	
		Latitude ϕ (N)	Longitude λ (E)
Grlja waterfall, 5 May 2017	992	42° 34’ 07"	19° 49’ 43"
Sušica River Canyon, 7 May 2017 and 3 June 2017	1.180	43° 11’ 46"	19° 00’ 18"
Podgorica, Cijevna River Canyon, 9 May 2017	38	42° 22’ 50"	19° 16’ 28"
Podgorica, Ćemovsko polje, 2 June 2017	76	42° 24’ 34"	19° 19’ 51"
Žabljak, 5 June 2017	1.450	43° 09’ 04"	19° 07’ 54"
Komarnica, Nevidio, 6 May 2017	968	42° 59’ 27"	19° 04’ 03"
Pljevlja, Ćehotina, 10 May 2017	671	43° 23’ 20"	19° 10’ 38"
Durmitor Mt., Goveđe jezero Lake, 6 June 2017	1520	43° 11’ 27"	19° 06’ 01"
Žabljak, Meždo, 21 July 2017	1.376	43° 08’ 52"	19° 09’ 09"
Durmitor Mt., Veliki Štuoc, 22 July 2017	1.930	43° 11’ 08"	19° 03’ 46"
Kom Vasojevićki Mt., Trešnjevik, 23 August 2018.	1.303	42° 44’ 14"	19° 41’ 41"
Gusinje, Savini izvori (= Alipašini izvori), 25 June 2018	918	42° 32’ 41"	19° 49’ 28"
Bioč Mt., 10 July 2018 and 18 July 2018.	1.190	43° 11’ 02"	18° 43’ 51"
Maglić Mt., 11 July 2018	1.287	43° 15’ 40"	18° 46’ 14"
Bjelasica Mt., Jakovača, 15 July 2019	1.673	42° 51’ 27"	19° 42’ 03"
Mratinje, 21 July 2019	780	43° 15’ 58"	18° 48’ 19"
Obzir Mt., Meštrovac, 24 July 2019	1.419	43° 17’ 07"	19° 02’ 29"
Bijela Gora, Orjen Mt., 28 June 2020	974	42° 39’ 05"	18° 36’ 09"
Subra, Orjen Mt., 30 June 2020	1.167	42° 30’ 46"	18° 33’ 16"
Kutska Rijeka, Cecune, Andrijevica, 9 July 2020	954	42° 38’ 41"	19° 47’ 08"

one female; Orijen Mt., Bijela Gora, 974 m, 28 June 2020., one female. (Fig. 1). Genitalia checked, slide DU-2935.

Figure 2. *Satyrium spini* f *albosparsa* Oberthür, 1910).

Pyrausta nigrata (Scopoli, 1763), Komarnica, Nevidio, 968 m, 6 May 2017, one male.

Sitochroa verticalis (Linnaeus, 1758), Pljevlja, Ćehotina, 671 m, 10 May 2017, two males

Anania funebris (Ström, 1768), Durmitor Mt., Sušica River Canyon, 1180 m, 3 June 2017, one female.

Family Lycaenidae Leach, 1815

Satyrium spini f albosparsa Oberthür, 1910, Gusinje, Savini izvori (= Alipašini izvori), 918 m, 25 June 2018. (Fig. 2)

In this aberration the usual white line on the undersides of the wings has been expanded into a broad white band Tutt (1914).

Figure 3. *Leptotes pirithous* Linnaeus, 1767.

Leptotes pirithous Linnaeus, 1767. Kutska Rijeka, Cecune, 954 m, Andrijevica, 9 Juli 2020. Female laying eggs. (Fig. 3)

Phengaris arion (Linnaeus, 1758), Maglić Mt., 1287 m, 11 July 2018, one female.

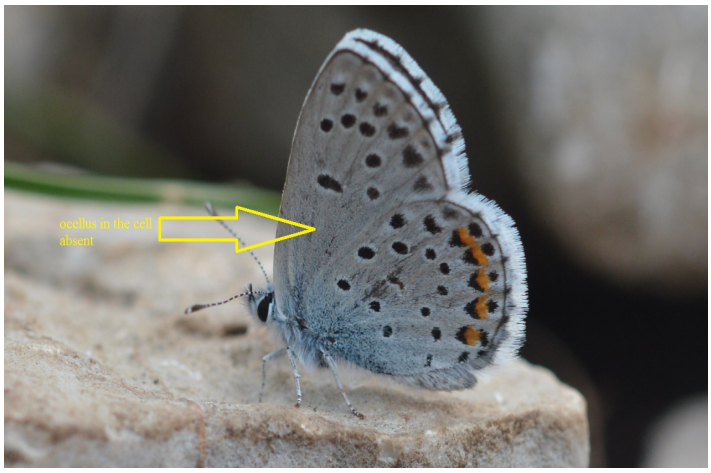

Figure 4. *Pseudophilotes vicrama schiffermuelleri* (Hemming, 1929).

Figure 5. *Erebia alberganus* (De Prunner, 1798).

Pseudophilotes vicrama schiffermuelleri (Hemming, 1929), Orjen Mt., Subra, 1167 m, 30 June 2020 (Fig. 4).

A specimen which lacked the usual basal ocellus of the typical form was recorded. There appears to be no name for this aberration Todisco et al. (2018).

Family Nymphalidae Rafinesque, 1815

Erebia alberganus (De Prunner, 1798), Bjelasica Mt., Jakovača, 1673 m, 15 July 2019, one female. (Figs. 5 & 6).

Erebia alberganus, first named by de Prunner in 1798, is named *E. albergana* by some authorities, eg Kudrna et al. (2015), following the Latin rule of adjectival agreement with the grammatical gender of the generic name. Franeta (2018) places *E. alberganus* as new to Montenegro, recorded by him in the Čakor Pass on 17 July 2017. However, Kudrna et al. (2015) had already noted this species in Montenegro. So, our finding on Bjelasica Mt. is the third record for this species in Montenegro.

Figure 6. *Erebia alberganus* (De Prunner, 1798).

Erebia alberganus would appear to be a relict species, restricted, as it is, to warm grasslands and meadows, often sheltered by woodland, in mountainous regions Tolman & Lewington (2008). Thus it is found extensively in the Alps, but also exhibits a somewhat disjunct distribution overall, in the Apennine Mountains of Italy, the Cantabrian Mountains of N Spain and several isolated localities in the Balkans.

Figure 7. *Melanargia galathea* ab. *nigrata* Schröder, 1924.

Melanargia galathea ab. nigrata Schröder, 1924, Obzir Mt., Meštrovac, 1419 m, 24 July 2019, one male (Figs. 7 & 8).

This is a form which exhibits all-black forewings and ..."the hindwings equally darkened; only the pale basal patch and (pale) central band of patches stand out, although they are strongly blackish darkened. Frohawk's f *nigra* would appear to be to be the same form" Goodson & Read (1930-1950).

Family Lasiocampidae Harris, 1841

Malacosoma castrensis (Linnaeus, 1758), Mratinje, 780 m, 21 July 2019, one female.

Family Geometridae Leach, 1815

Colostygia aptata (Hübner, [1813]), Durmitor Mt., Žabljak, Meždo, 1387 m, 21 July 2017, one male. (Fig. 9)

Figure 8. *Melanargia galathea* ab. *nigrata* Schröder, 1924.

Figure 9. *Colostygia aptata* (Hübner, [1813]).

Widely distributed across the Palaearctic and has previously been found in other localities in the Balkans. This is a moth of dry, rocky, sunny grassland slopes and the fringes of forests, with poor soil, on mountains. The larvae feed on *Galium* spp Skou & Sihvonen (2015).

Already known species in Montenegro from several localities Tomić et al. (1990), but a very rare species.

Chesias rufata pinkeri Schawerda (1939), Durmitor Mt., Žabljak, 1450 m, 5 June 2017, one male. Genitalia checked, slide CG-2922.

Chesias rufata is a relatively common species, found locally across much of Europe, south of Scotland and Sweden, and also in North Africa. *C. rufata pinkeri* was originally believed to be a separate species, (Schawerda (1939), described on the basis of material from Ohrid in North Macedonia), and was later seen as a synonym of *rufata*; but it is now understood as a subspecies Hausman & Viidalepp (2012). *C.r. pinkeri* has been found sparingly across the western and southern Balkans. It is to be found on dry, open karst areas, where the larvae will feed on *Cytisus scoparius* or *Genista* spp. This is the second record of this taxon in Montenegro.

Hypoxystis pluviaria (Fabricius, 1787), Sušica River Canyon, 1180 m, 7 May 2017, two males, one female. Genitalia checked, slide CG-2894. (Fig. 10)

Figure 10. *Hypoxystis pluviaria* (Fabricius, 1787).

Distributed in Sweden and Finland and also eastern Europe to Siberia and Mongolia. Already known from Bosnia & Herzegovina and Republic of North Macedonia. This is a moth of wetlands, damp meadows, damp deciduous woodlands and woodland clearings, mostly at lower altitudes. The larvae are oligophagus, feeding on *Galium palustre, Cytisus scoparius, Senecio jacobaeae* and *Senecio nemorensis*. A new species for Montenegro.

Aspitates ochrearia (Rossi, 1794), Podgorica, Cijevna River Canyon, 38 m, 9 May 2017, one male.

Distributed in western and southern Europe. Already known from Bosnia & Herzegovina. The habitat of this moth is dry grasslands and dunes. The larvae eat a number of low-growing plants, including *Daucus carota, Plantago cornopus, Ononis* spp, *Linaria* spp, *Artimesia* spp, *Vicia tetrasperma* and *Crepis vesicaria*. A new species for Montenegro. (Fig. 11).

Figure 11. *Aspitates ochrearia* (Rossi, 1794).

Family Erebidae Leach, 1815

Eilema pygmaeola (Doubleday, 1847), Durmitor Mt., Veliki Štuoc, 1930 m, 22 July 2017, one male. Genitalia checked, slide CG-2904 (Fig. 12).

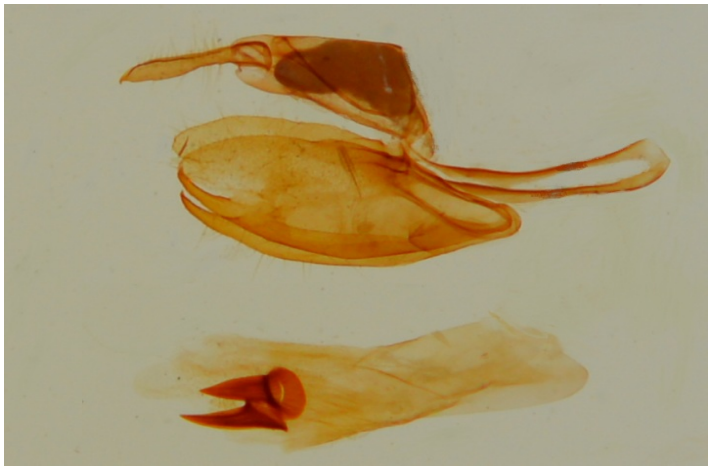

Figure 12. *Eilema pygmaeola* (Doubleday, 1847).

Epatolmis luctifera ([Denis & Schiffermüller], 1775), Bioč Mt., 1190 m, 10 July 2018, one male.

REFERENCES

Domingo, J., Huemer, P., & Baixeras, J. 2003, *Ethmia penyagolosella* sp. n. (Lepidoptera: Ethmiidae), a new species from Spain. Nachrichten des entomologischen Vereins Apollo, [2] 24(4), pp. 183-188.

Franeta, F. 2018, Checklist of the butterflies (Lepidoptera: Papilionoidea) of Montenegro. Zootaxa, 4392 (1), pp. 128-148.

Goodson, A. & Read, D. 1930-1950, Aberrational and subspecific forms of British Lepidoptera. Volumes 1-12 and 1 addenda volume [typescript]. Natural history Museum, London.

Hausman, A. & Viidalepp, J. 2012, The Geometrid Moths of Europe. Vol. 3 Subfamily Larentiinae I. Apollo Books.

Kudrna, O., Pennerstorfer, J., & Lux, K. 2015, Distribution Atlas of European Butterflies and Skippers. Wissenschaftlicher Verlag Peks.

Nieukerken, v. J. 2011, In: Zhang, Z. Z. (Ed) Animal biodiversita. An outline of higher-level classification and survey of taxonomic richness. Zootaxa, 3148, pp. 1-237.

Schawerda, K. 1939, *Chesias züllichi* Schaw. und Chesias pinker Schaw., species novae. CZeitschrift des Österreichischen Entomologischen Vereins, 24, pp. 145-147.

Skou, P. & Sihvonen, P. 2015, The Geometrid Moths of Europe. Vol. 5 Subfamily Ennominae I. Brill, Leiden.

Todisco, V., Grill, A., Fiedler, K., et al. 2018, Molecular phylogeny of the Palaearctic butterfly genus *Pseudophilotes* (Lepidoptera: Lycaenidae) with focus on the Sardinian endemic P. barbagiae. Zoology, 3(4), pp. 1-11.

Tolman, T. & Lewington, R. 2008, Collins Butterfly Guide. Harper Collin Publisher, London.

Tomić, D., Vasić, K., Carnelutti, J., Zečević, M., & Kranjčev, R. 1990, Heterocera II. Geometridae (Insecta, Lepidoptera). In: Fauna Durmitora, Sveska 3. Crnogorska akademija nauka i umjetnosti, Posebna izdanja knj. 23, Odeljenje prirodnih nauka, knjiga 14, Titograd [Podgorica], pp. 159-202.

Tutt. 1914, A natural history of the British butterflies, their worldwide variation and geographical distribution. 4-8+373 pp., 44 pls.; Eliot Stock, London.

Wiemers, M. 2018, An updated checklist of the European Butterflies (Lepidoptera, Papilionoidea). ZooKeys, 811, pp. 9-45.

Bulletin of Natural Sciences Research
Vol. 11, No. 2, 2021, pp. 13-19.

DOI: https://doi.org/10.5937/bnsr11-30426
Original Scientific Paper

ULTRASOUND-ASSISTED SYNTHESIS OF NOVEL 3-(PYRIDINYLAMINO)-1-FERROCENYLPROPAN-1-ONES

ALEKSANDRA MINIĆ JANČIĆ[1*], DANIJELA ILIĆ KOMATINA[1], ANKA TODOSIJEVIĆ[2] DRAGANA STEVANOVIĆ[3]

[1]Faculty of Technical Sciences, University of Priština in Kosovska Mitrovica, Kosovska Mitrovica, Serbia
[2]Faculty of Agriculture, University of Niš, Kruševac, Serbia
[3]Faculty of Science, University of Kragujevac, Kragujevac, Serbia

ABSTRACT

In this work we will report the formulation of novel 3-(pyridinylamino)-1-ferrocenylpropan-1-ones. A fruitful aza-*Michael* addition of pyridinamine moiety to a conjugated enone, 1-ferrocenylpropenone, has been accomplished by an ultrasonic irradiation of the mixture of these reactants. As the catalyst montmorillonite K-10 has been used and the reaction has been carried out as solvent-free, yielding ferrocene containing *Mannich bases*, compounds considered as important precursors in organic synthesis. The reaction score has been evaluated on three examples. The prepared products have been purified by column chromatography. In addition, a detailed characterization of the obtained 3-(pyridin-2-ylamino)-1-ferrocenylpropan-1-on and 3-(pyridin-3-ylamino)-1-ferrocenylpropan-1-on has been completed by IR and NMR spectroscopy, as well as elemental analyses.

Keywords: aza-*Michael* addition, Ultrasound irradiation, 3-(pyridinylamino)-1-ferrocenylpropan-ones, Mannich bases, Spectral characterization.

INTRODUCTION

Ferrocene has been discovered in 1951 (Kealy & Pauson, 1951), and since then its derivatives have been found applications in many areas, among which the most important are in material science, asymmetric catalysis, bioorganometallic chemistry, medicinal chemistry, and organic synthesis (Köpf-Maier et al., 1984; Houlton et al., 1991; Kowalski, 2018). The application of ferrocene derivatives in the medicinal investigations proved to be a fertile area of bioorganometallic chemistry. Although ferrocene is not biologically active, it possesses a unique feature to strongly affect the activity of the structures to which is bound for (Togni, 1996). The incorporation of ferrocene nucleus into biologically relevant molecules can significantly enhance molecular properties such as solubility, hydrophobicity, and lipophilicity of ''parent compounds'' (Jaouen, 2006; Gambino & Otero, 2012; Salas et al., 2013; Biot et al., 2012; Supan et al., 2012). In such a way, some ferrocenyl derivatives like ferroquine and ferrocifen occupied an important position in pharmaceutical and medicinal chemistry. Likewise, the presence of the organoiron unit in bioactive skeletons increases their original antimalarial and antitumoral activity. Thus, the ferrocene moiety was recognized as an attractive pharmacophore in drug design (N'Da, & Smith, 2014) and a multitude of reports dealing with derivatives of this metallocene have been appeared in the literature.

In continuation of our long-standing interest in the synthesis of novel Fc-containing (Fc = ferrocene) heterocyclic compounds, of potential biological interest (Pejović et al., 2012a; Pejović et al., 2017; Pejović et al., 2018a; Pejović et al., 2018b), and in design and optimizations of reactions conditions, we reported synthesis of bioactive 2-ferrocenoyl ethyl aryl amines and 1-ferrocenyl-3-(quinolinylamino)propan-1-ones, as it is presented on Scheme 1., (Damljanović et al., 2011; Pejović et al., 2012b; Minić et al., 2020a). These Mannich bases have been proved to be an excellent starting material for the synthesis of Fc derivatives (Minić et al., 2020a; Minić et al., 2015; Minić et al., 2017; Minić et al., 2018; Minić et al., 2019; Minić et al., 2020b; Pejović et al., 2015). Hence, the synthesis and spectral characterization of novel *Mannich bases* bearing ferrocenyl group and pyridinamine ring gained in this manner could be of great interest.

In agreement with above statement, herein, we report the ultrasound-assisted synthesis between three different pyridinamine and 1-ferrocenylpropenone. All formulated compounds have been washed by column chromatography and their predicted structure have been verified with spectroscopic data (^{1}H-NMR, ^{13}C-NMR, and IR), as well as by elemental analyses. Also, this synthetic approach gives rise to favorable starting materials for advance synthesis of Fc-containing compounds.

EXPERIMENTAL

Materials and measurements

All chemicals were commercially available and used as received, except the solvents, which were purified by distillation. Ultrasonic cleaner Elmasonic S 10 (Elma, Germany), 30W was used for the ultrasonically supported synthesis. Chromatographic

* Corresponding author: aleksandra.minic@pr.ac.rs

separations were carried out using silica gel 60 (Merck, 230–400 mesh ASTM), whereas silica gel 60 on Al plates, (Merck, layer thickness 0.2 mm) was used for TLC. Melting points were determined on a Mel-Temp capillary melting points apparatus, model 1001, and the given values have been uncorrected. The ^{1}H- and ^{13}C-NMR spectra of the samples in $CDCl_3$ have been recorded on a Varian Gemini (^{1}H- at 200 MHz, ^{13}C- at 50 MHz) NMR spectrometer. Chemical shifts are reported in ppm (δ) values relative to TMS (δ_H 0 ppm) in ^{1}H-, ^{13}C-NMR spectra. The coupling constants (J) are reported in Hz. Multiplicities of proton resonance are designated as singlet (s), a doublet (d), a doublet of doublets (dd), a triplet (t), a pseudo triplet (*pseudo* t), doublet of doublets of doublets (ddd), a quartet (q) and a multiplets (m). IR measurements were carried out with a Perkin–Elmer FTIR 31725-X spectrophotometer. Microanalyses of carbon, hydrogen and nitrogen were carried out with a Carlo Erba 1106 model microanalyzer; these results agreed satisfactorily with the calculated values.

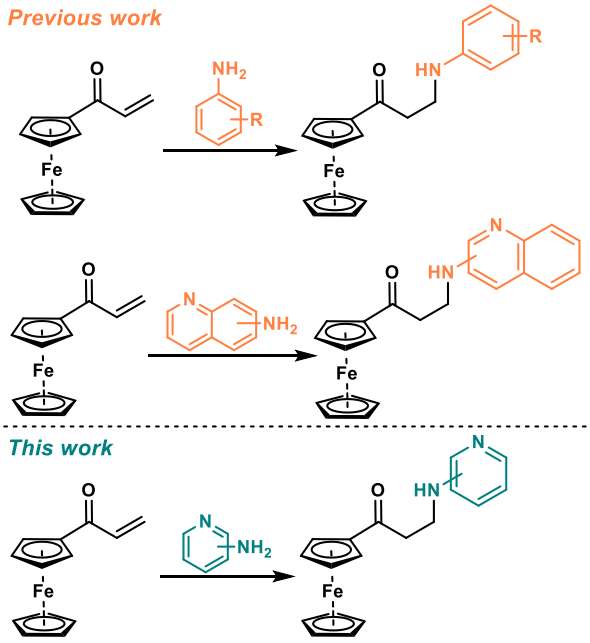

Scheme 1. Synthesis of various *Mannich bases* bearing ferrocenyl group.

Synthesis and spectral characterization

*General procedure for the synthesis of 3-(pyridinylamino)-1-ferrocenylpropan-1-ones (**3a-c**)*

The 3-(pyridinylamino)-1-ferrocenylpropan-1-ones (**3a-c**) have been prepared following slightly modified formerly reported procedure (Pejović et al., 2012b; Minić et al., 2015; Minić et al., 2017; Minić et al., 2018; Minić et al., 2019). A test tube containing a well homogenized mixture of 1-ferrocenylpropenone (240 mg, 1 mmol), the analogous pyridinamine (**2a-c**, 2 mmol) and montmorillonite K-10 (100 mg, 0.42 m-eq.) has been placed in the ultrasonic cleaner for irradiations and the reaction outcome has been checked by TLC. Later, CH_2Cl_2 (10 ml) was added to the mixture, and the contents were filtered off. The solid residue was filtrated with water and brine, as well as dried over anh. Na_2SO_4. overnight. After the evaporation of the solvent, the crude mixture has been separated by chromatography on a SiO_2 column. The corresponding 3-(pyridinylamino)-1-ferrocenylpropan-1-ones (**3a-c**) have been washed from the column by a mixture of hexane and MeOH 9 : 1 (v/v). The obtained spectral data for 3-(pyridinylamino)-1-ferrocenylpropan-1-ones follow.

3-(Pyridin-2-ylamino)-1-ferrocenylpropan-1-on (***3a***). Dark red solid; mp 134 °C. Yield 60%. ^{1}H NMR (200 MHz, $CDCl_3$) δ = 8.11 (dd, J = 5.1, 1.1 Hz, 1H, H-3'), 7.37 (ddd, J = 8.9, 7.1, 1.9 Hz, 1H, H-4'), 6.54 (ddd, J = 7.1, 5.1, 0.8 Hz, 1H, H-5'), 6.41 (d, J = 8.4 Hz, 1H, H-6'), 5.06 (s, 1H, NH), 4.77 (pseudo t, J = 1.9 Hz, 2H, H-4" and H-5"), 4.49 (pseudo t, J = 1.9 Hz, 2H, H-2" and H-3"), 4.10 (s, 5H, H-1"'), 3.77 (q, J = 6.1 Hz, 2H, H-3a and H-3b), 3.07 (t, J = 5.9 Hz, 2H, H-2a and H-2b). ^{13}C NMR (50 MHz, $CDCl_3$) δ = 203.6 (C-1), 158.3 (C'), 147.9 (C'), 137.2 (C'), 112.7 (C'), 108.1 (C'), 78.9 (C"), 72.3 (C"), 69.7 (C"'), 69.2 (C"), 38.7 (C-3), 36.7 (C-2).IR (ATR, cm^{-1}): ν = 3200 (N-H) cm^{-1}; ν = 1671 (C=O) cm^{-1}. Anal. Calc. for $C_{18}H_{18}FeN_2O$: C, 64.69; H, 5.43; Fe, 16.71; N, 8.38; O, 4.79. Found: C, 64.71; H, 5.41; N, 8.36 %.

3-(Pyridin-3-ylamino)-1-ferrocenylpropan-on (***3b***). Dark red solid; mp 92 °C. Yield 75%. ^{1}H NMR (200 MHz, $CDCl_3$) δ 8.08 = (d, J = 2.6 Hz, 1H, H-2'), 7.96 (d, J = 4.5 Hz, 1H, H-4'), 7.09 (dd, J = 8.3, 4.5 Hz, 1H, H-5'), 6.92 (d, J = 8.2 Hz, 1H, H-6'), 4.77 (pseudo t, J = 1.8 Hz, 2H, H-4" and H-5"), 4.53 – 4.48 (overlapped m, 3H, H-2", H-3" and NH), 4.12 (s, 5H, H-1"'), 3.57 (q, J = 5.6 Hz, 2H, H-3a and H-3b), 3.02 (t, J = 6.0 Hz, 2H, H-2a and H-2b). ^{13}C NMR (50 MHz, $CDCl_3$) δ = 203.0 (C-1), 143.6 (C'), 138.7 (C'), 135.9 (C'), 123.6 (C'), 118.7 (C'), 78.5 (C"), 72.4 (C"), 69.7 (C"'), 69.1 (C"), 38.3 (C-3), 37.9 (C-2). IR (ATR, cm^{-1}): ν = 3211 (N-H) cm^{-1}; ν = 1665 (C=O) cm^{-1}. Anal. Calc. for $C_{18}H_{18}FeN_2O$: C, 64.69; H, 5.43; Fe, 16.71; N, 8.38; O, 4.79. Found: C, 64.70; H, 5.40; N, 8.40 %.

RESULTS AND DISCUSSION

Synthesis

As it has been declared in the introduction in the last decade our research group stated reaction conditions for the synthesis of 3-arylamino-1-ferrocenylpropan-1-ones in high yields. This reaction has yielded numerous compounds, which have been demonstrated to be both biological active agents and excellent starting materials (Damljanović et al., 2011; Pejović et al., 2012b; Minić et al., 2015; Minić et al., 2017; Minić et al., 2018; Minić et al., 2019; Minić et al., 2020a), see Scheme 1. Consequently, for required synthesis within this work we agreed to apply these already know reaction conditions (see Scheme 2). A test tube containing a well homogenized mix of 1-ferrocenylpropenone (240 mg, 1 mmol), the analogous pyridinamine (**2a**, 2 mmol) and montmorillonite K-10 (100 mg,

0.42 m-eq.) has been placed in the ultrasonic cleaner for 1h irradiations in the absence of solvent at ambient temperature. Later, the crude product has been purified by column chromatography (SiO_2/n-hexane–MeOH, 9 : 1, v/v) to give 3-(pyridin-2-ylamino)-1-ferrocenylpropan-1-on (**3a**) in only 10% yield. This result shows us that the reaction certainly occurs, but also that we need to and established the optimal parameters. Therefore, we set reaction under no different conditions, but this time reaction outcome has been monitored by TLC. Indeed, based on TLC plate, for the reaction to be fully done it was necessary much more time around 8 hours. Usual workup of the reaction and column chromatography (SiO_2/n-hexane–MeOH, 9 : 1, v/v), provided compound **3a** in 60% yield based on 1-ferrocenylpropenone.

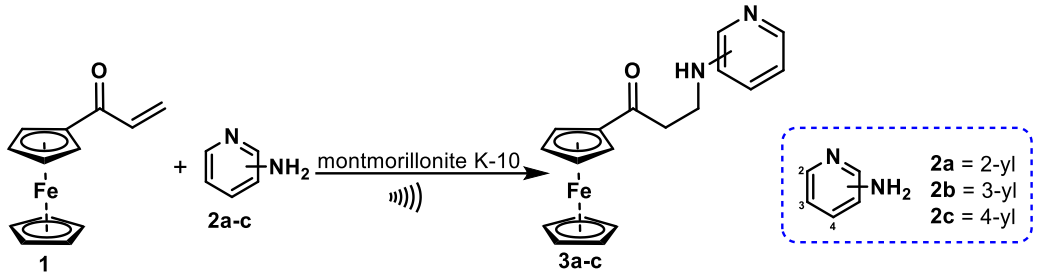

Scheme 2. Synthesis of novel 3-(pyridinylamino)-1-ferrocenylpropan-1-ones (**3a-c**).

Reaction score has been evaluated on two additional examples and we discovered very interesting results (see Table 1). Under submitted conditions 3-(pyridin-3-ylamino)-1-ferrocenylpropan-1-on (**3b**) has been smoothly prepared in good yield 75% (see Table 1, entry 2), but when we used pyridine-4-amine as starting substrate the reaction has not proceed (see Table 1, entry 3). The explanation for these outcomes must be the different influence of electronic properties depending on the position of nitrogen atom in pyridinamine ring.

Table 1. Substrate scope for the production of 3-(pyridinylamino)-1-ferrocenylpropan-1-ones (**3a-c**)

Entry	Starting substrate	Time (h)	Product	Yield (%)[c]
1	pyridin-2-amine (**2a**)	8	**3a**	60
2	pyridin-3-amine (**2b**)	6	**3b**	75
3	pyridin-4-amine (**2c**)	10	**3c**	/

Spectral characterization

The newly obtained compounds **3a** and **3b** described in this paper have been found to be stable at the ambient temperature for a prolonged time and could safely be handled in air, but like other Fc derivatives, they should be stored in closed containers. To validate their structure detailed characterized by standard spectroscopic techniques (IR, ^{1}H- and ^{13}C-NMR), as well as elemental analyses has been done. All spectral data were completely consistent with the planned structures (for more data see Experimental part).

The IR spectra of compounds **3a** and **3b** contained characteristic vibrations of the N-H bonds at 3234 cm^{-1}. The strong band at 1670 cm^{-1} relating to absorptions of the C=O bond. Three sets of signals have been observed in the ^{1}H-NMR spectra. The first belongs to protons of the methylene groups, the second to protons of the ferrocene moiety and the third to the aromatic protons (see Figure 1).

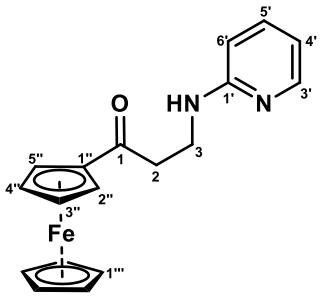

Figure 1. Labeled carbons atoms for NMR characterization.

The signals at ~ 3.57–3.77 and 3.02–3.07 ppm come from the protons of the methylene groups (H-3a, H-3b, H-2a, and H-2b, respectively). The broad singlets at ~ 5.06 ppm has been assigned to the NH protons. Likewise, the ^{1}H-NMR data for the newly produced compound **3a** and **3b** has been conventional for monosubstituted ferrocene (a typical intensity pattern of 2 : 2 : 5 for the H-atoms of Fc). Pseudo triplets at 4.48–4.77 ppm originate from the protons of the substituted cyclopentadiene rings (H-2'', H-3'', H-4'' and H-5''), and the singlets at ~ 4.10 ppm belong to the H-atoms of unsubstituted ferrocene cyclopentadiene rings (H-1'''). The signals of aromatic protons (H-2', H-3', H-4', H-5' and H-6') are positioned at the predicted chemical shifts (> 6.40 ppm) (for more data see Experimental part, Figure 2 and Figure 3).

Supplementary, signals assigned to the corresponding carbons of the synthesized compounds **3a** and **3b** appear in the expected regions of the ^{13}C NMR spectra. The corresponding signals originated from the carbonyl group (δ(C) around 203 ppm), aromatic core above 108 ppm, ferrocene moiety between 69 and 79 ppm and aliphatic carbons at *ca* 37 ppm. (for more data see Experimental part, Figure 4, and Figure 5).

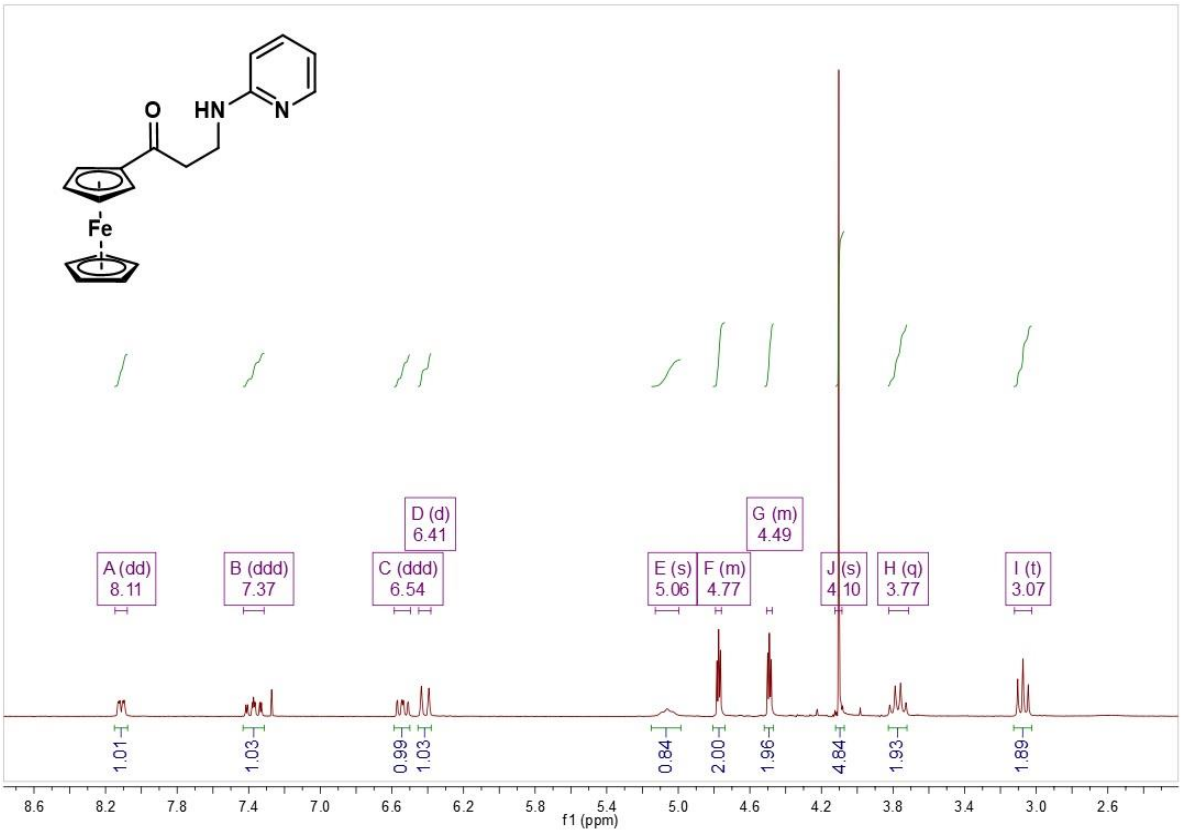

Figure 2. ^{1}H NMR (200 MHz, $CDCl_3$) spectrum of **3a.**

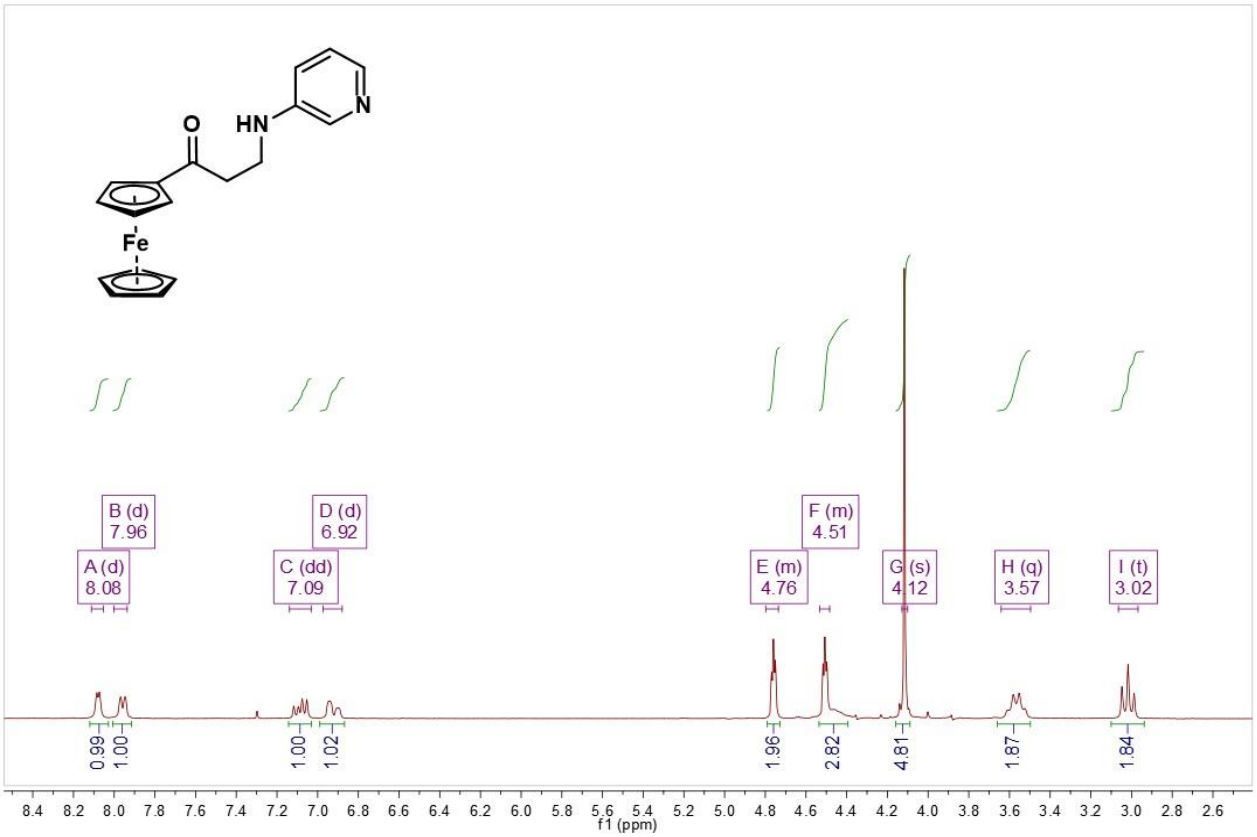

Figure 3. ^{1}H NMR (200 MHz, $CDCl_3$) spectrum of **3b.**

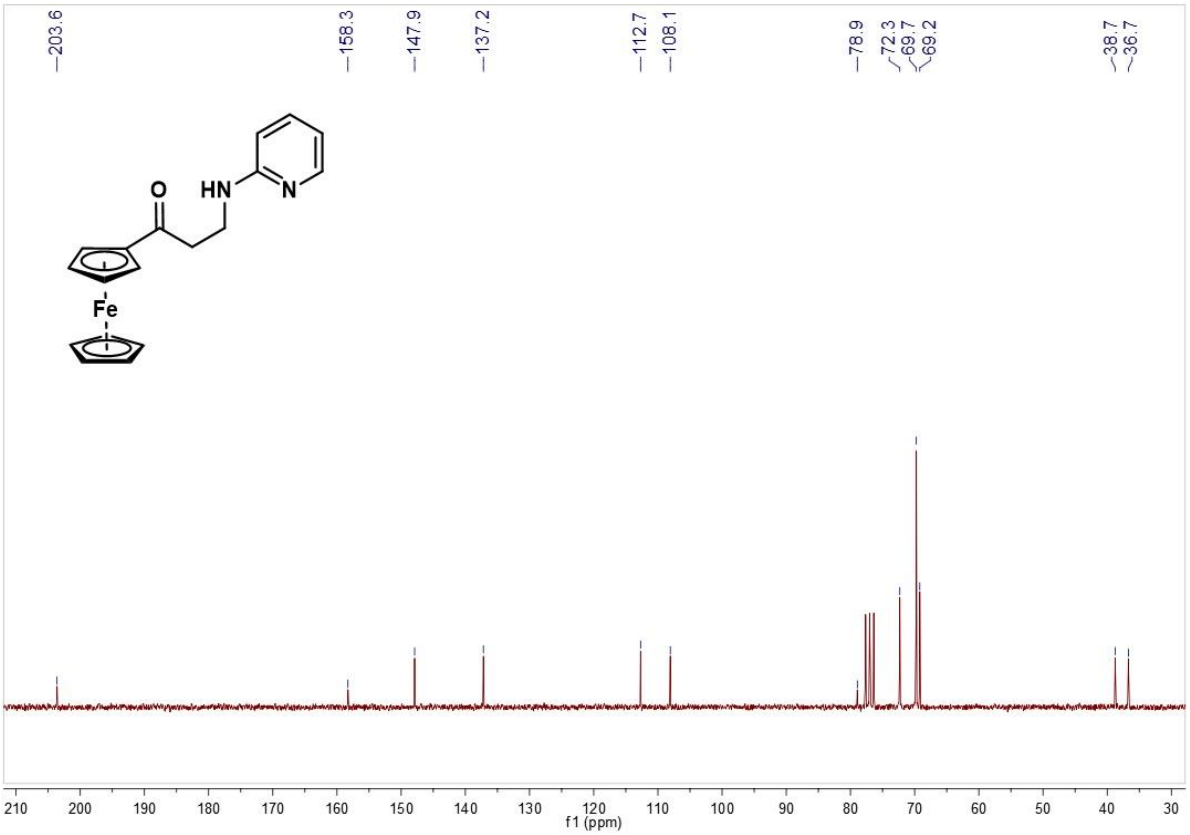

Figure 4. ^{13}C NMR (50 MHz, $CDCl_3$) spectrum of **3a.**

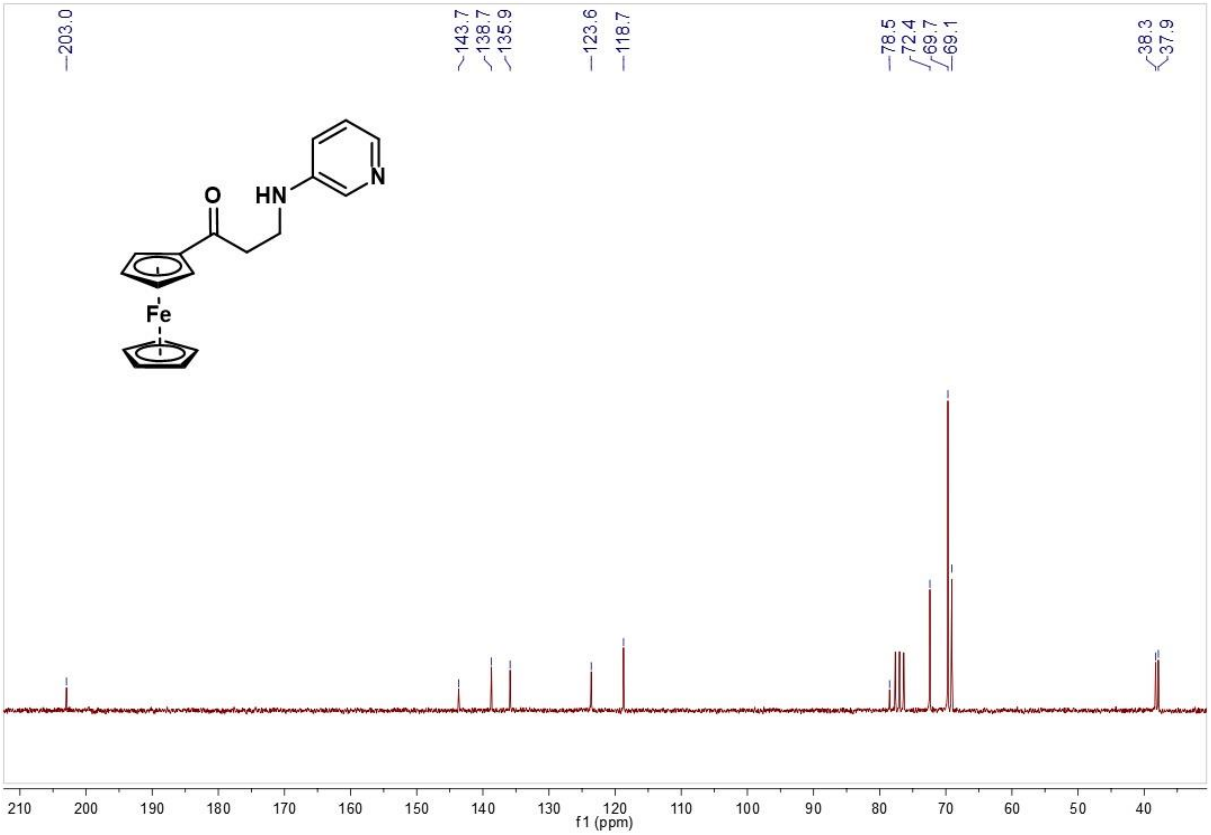

Figure 5. ^{13}C NMR (50 MHz, $CDCl_3$) spectrum of **3b.**

CONCLUSION

In a nutshell, within this study first time synthesis of 3-(pyridin-2-ylamino)-1-ferrocenylpropan-1-on and 3-(pyridin-3-ylamino)-1-ferrocenylpropan-1-on has been submitted. Proposed structures of prepared molecules were undoubtedly confirmed by spectroscopic techniques (IR and NMR), as well as by elemental analyses. Added investigation to broaden this methodology for the synthesis of other ferrocenes is under development of our research group. In supplement, the synthesized molecules correspond to be interesting starting material for biological evaluation.

ACKNOWLEDGMENTS

This work was supported by the Ministry of Education, Science and Technological development of the Republic of Serbia (Agreement No. 451-03-68/2020-14/200122).

REFERENCES

Biot, C., Castro, W., Botte, C. Y. & Navarro, M. 2012. The therapeutic potential of metal-based antimalarial agents: Implications for the mechanism of action. Dalton Transactions, 41, pp. 6335-6349. doi.10.1039/C2DT12247B

Damljanović, I., Stevanović, D., Pejović, A., Vukićević, M., Novaković, S. B., Bogdanović, G. A., Mihajilov-Krstev, M. T., Radulović, N. & Vukićević, R. D. 2011. Antibacterial 3-(arylamino)-1-ferrocenylpropan-1-ones: Synthesis, spectral, electrochemical and structural characterization. Journal of Organometallic Chemistry, 696, pp. 3703-3713. doi.org/10.1016/j.jorganchem.2011.08.016

Gambino, D. & Otero, L. 2012. Perspectives on what ruthenium-based compounds could offer in the development of potential antiparasitic drugs. Inorganica Chimica Acta, 393, pp. 103–114. doi.10.1016/j.ica.2012.05.028

Houlton, A., Roberts, R. M. G. & Silver, J. 1991. Studies on the anti-tumour activity of some iron sandwich compounds. Journal of Organometallic Chemistry, 418, pp. 107-112. doi.org/10.1016/0022-328X(91)86350-Y

Jaouen, G. 2006. Bioorganometallics: Biomolecules, Labeling, Medicine, John Wiley.

Kealy, T. J. & Pauson, P. L. 1951. A New Type of Organo-Iron Compound. Nature, 168, pp. 1039-1040. DOI:10.1038/1681039b0

Köpf-Maier, P., Köpf, H. & Neuse, E. W. 1984. Ferrocenium Salts—The First Antineoplastic Iron Compounds. Angewandte Chemie International Edition in English, 23, pp. 456-457. doi.org/10.1002/anie.198404561

Kowalski, K. 2018. Recent developments in the chemistry of ferrocenyl secondary natural product conjugates. Coordination Chemistry Reviews, 366, pp. 91-108. doi.org/10.1016/j.ccr.2018.04.008

Minić, A., Stevanović, D., Damljanović, I., Pejović, A., Vukićević, M., Bogdanović, G. A., Radulović, N. & Vukićević, R. D. 2015. Synthesis of ferrocene-containing six-membered cyclic ureas via α-ferrocenyl carbocations. RSC Advances, 5, pp. 24915-24919. doi. 10.1039/C5RA01383F

Minić, A., Stevanović, D., Vukićević, M., Bogdanović, G. A., D'hooghe, M., Radulović, N. & Vukićević, R. D. 2017. Synthesis of novel 4-ferrocenyl-1,2,3,4-tetrahydroquinolines and 4-ferrocenylquinolines via α-ferrocenyl carbenium ions as key intermediates. Tetrahedron, 73, pp 6268-6274. doi. 10.1016/j.tet.2017.09.014

Minić, A., Bugarinović, J., Ilić-Komatina, D., Bogdanović, G. A., Damljanović, I. & Stevanović, D. 2018. Synthesis of novel ferrocene-containing 1,3-thiazinan-2-imines: One-pot reaction promoted by ultrasound irradiation. Tetrahedron Letters, 59, pp. 3499-3502. doi. 10.1016/j.tetlet.2018.08.029

Minić, A., Bugarinović, J., Pešić, M., & Ilić-Komatina, D. 2019. Novel 4-ferrocenyl-8-(phenylthio)-1,2,3,4-tetrahydroquinoline: design, synthesis and spectral characterization, UNIVERSITY THOUGHT - Publication in Natural Sciences, 9. DOI:10.5937/univtho9-20839.

Minić, A., Van de Walle, T., Van Hecke, K., Combrinck, J., Smith, P. J., Chibale, K. & D'hooghe, M. 2020a. Design and synthesis of novel ferrocene-quinoline conjugates and evaluation of their electrochemical and antiplasmodium properties, European Journal of Medicinal Chemistry, 187, pp. 111963. https://doi.org/10.1016/j.ejmech.2019.111963

Minić, A., Novaković, S. B., Bogdanović, G. A., Bugarinović, J., Pešić, M., Todosijević, A., Ilić-Komatina, D., Damljanović, I. & Stevanović, D. 2020b. Synthesis and structural characterizations of novel atropoisomeric ferrocene-containing six-membered cyclic ureas, Polyhedron, 177 pp. 114316. https://doi.org/10.1016/j.poly.2019.114316

N'Da, D & Smith, P. 2014. Synthesis, in vitro antiplasmodial and antiproliferative activities of a series of quinoline–ferrocene hybrids. Medicinal Chemistry Research, 23, pp. 1214-1224. doi.org/10.1007/s00044-013-0748-4

Pejović, A., Damljanović, I., Stevanović, D., Vukićević, M., Novaković, S. B., Bogdanović, G. A., Radulović, N. & Vukićević, R. D. 2012a. Antimicrobial ferrocene containing quinolinones: Synthesis, spectral, electrochemical and structural characterization of 2-ferrocenyl-2,3-dihydroquinolin-4(*1H*)-one and its 6-chloro and 6-bromo derivatives, Polyhedron, 31, pp. 789-795. https://doi.org/10.1016/j.poly.2011.11.006

Pejović, A., Stevanović, D., Damljanović, I., Vukićević, M., Novaković, S. B., Bogdanović, G. A., Mihajilov-Krstev, M. T., Radulović, N. & Vukićević, R. D. 2012a. Ultrasound-assisted synthesis of 3-(arylamino)-1-ferrocenylpropan-1-ones. Helvetica Chimica Acta, 95, pp. 1425-1441. doi.org/10.1002/hlca.201200009

Pejović, A., Danneels, B., Desmet, T., Cham, B. T., Nguyen, T., Radulović, N. S., Vukićević, R. D. & D'hooghe, M. 2015. Synthesis and Antimicrobial/Cytotoxic Assessment of Ferrocenyl Oxazinanes, Oxazinan-2-ones, and Tetrahydropyrimidin-2-ones, Synlett, 26, pp. 1195-1200. doi. 10.1055/s-0034-1380348

Pejović, A., Damljanović, I., Stevanović, D., Minić, A., Jovanović, J., Mihailović, V., Katanić, J. & Bogdanović, G. A. 2017. Synthesis, characterization and antimicrobial activity of novel ferrocene containing quinolines: 2-ferrocenyl-4-methoxyquinolines, 1-benzyl-2-ferrocenyl-2,3-dihydroquinolin-4(*1H*)-ones and 1-benzyl-2-ferrocenylquinolin-4(*1H*)-ones, Journal of Organometallic

Chemistry, 846, pp. 6-17. http://dx.doi.org/10.1016/j.jorganchem.2017.05.051

Pejović, A., Minić, A., Bugarinović, J., Pešić, M., Damljanović, I., Stevanović, D., Mihailović, V., Katanić, J., & Bogdanović, G. A. 2018a. Synthesis, characterization and antimicrobial activity of novel 3-ferrocenyl-2-pyrazolyl-1,3-thiazolidin-4-ones, Polyhedron, 155, pp. 382–389. https://doi.org/10.1016/j.poly.2018.08.071

Pejović, A., Minić, A., Jovanović, J., Pešić, M., Ilić Komatina, D., Damljanović, I., Stevanović, D., Mihailović, V., Katanić, J. & Bogdanović, G. A. 2018b. Synthesis, characterization, antioxidant and antimicrobial activity of novel 5-arylidene-2-ferrocenyl-1,3-thiazolidin-4-ones, Journal of Organometallic Chemistry, 869, pp. 1-10. https://doi.org/10.1016/j.jorganchem.2018.05.014

Salas, P. F., Herrmann, C. & Orvig, C. 2013. Metalloantimalarials. Chemical Reviews, 113, pp. 3450-3492. doi.10.1021/cr3001252

Supan, C., Mombo-Ngoma, G., Dal-Bianco, M. P., Salazar, C. L. O., Issifou, S., Mazuir, F., Filali-Ansary, A., Biot, C., Ter-Minassian, D., Ramharter, M., Kremsner, P.G. & Lell, B. 2012. Pharmacokinetics of Ferroquine, a Novel 4-Aminoquinoline, in Asymptomatic Carriers of Plasmodium falciparum Infections. Antimicrobial Agents and Chemotherapy, 56, pp. 3165–3173. doi. 10.1128/AAC.05359-11

Togni, A. 1996. Planar-Chiral Ferrocenes: Synthetic Methods and Applications. Angewandte Chemie International Edition in English, 35, pp. 1475-1477. doi.org/10.1002/anie.199614751

Bulletin of Natural Sciences Research
Vol. 11, No. 2, 2021, pp. 20-24.

DOI: https://doi.org/10.5937/bnsr11-29311
Original Scientific Paper

INFLUENCE OF THE ACIDITY OF THE IODOUS ACID SOLUTION SYSTEM ON THE KINETICS OF THE DISPROPORTIONATION REACTION

SMILJANA MARKOVIĆ [1*]

[1]Faculty of Technical Sciences, University of Priština in Kosovska Mitrovica, Kosovska Mitrovica, Serbia

ABSTRACT

Influence of the acidity of the iodous acid (HOIO) solution system on the kinetics disproportionation reaction is examined in aqueous sulfuric acid solution (0.125 moldm^{-3}). The disproportionation reaction rate constants were determined at 285, 291, 298 and 303 K based on data obtained under stationary conditions. The calculated rate constants increase with increasing temperature for different values of iodous acid and iodate concentrations. The average activation energy of 46 kJmol^{-1} was determined for the chosen temperature interval, by a graphical method. The values of *pseudo*-equilibrium concentrations of kinetically important and catalytic species H^+, H_2OI^+ i IO_3^- in the disproportionation reaction were determined for the given experimental conditions based on the equilibrium dissociation reactions of sulfuric and iodous acids in the quasi-stationary state. The estimated values of sulfuric and iodous acid are predominant and higher than the concentration of the protonated ion of H_2OI^+.

Keywords: Disproportionation reaction, Iodous acid, Activation energy, Rate constants, Kinetics.

INTRODUCTION

The iodous acid (HOIO) disproportionation reaction was studied under different experimental conditions in the visible and ultraviolet areas of the spectrum (Noszticzius et al., 1983; Lengyel et al., 1996; Urbansky et al., 1997). The theoretical approach and explanations of experimental results represent a significant contribution to chemical kinetics for analyses of systems in which the reaction occurs in iodine complex reactions (Mäkelä et al., 2002; O'Dowd et al., 2002; Jimenez et al., 2003; De Souza & Brown., 2014).

The mechanism of the process itself, which was studied in strong acidic aqueous solutions, is complex, slow and subject to autocatalysis (Lengyel et al., 1996). A detailed, complete mechanism of this complex dynamic process has not been fully determined yet. Namely, HOIO iodous acid decomposes in strong acidic aqueous solutions through a series of iodine-oxygen species that react with each other creating appropriate balances. Due to the complexity of the disproportionation, it is possible to followed only the reaction products that are produced during the reaction. The process depends upon the nature of the reacting species and solvents, as well as upon their acidity and temperature. High acidity is one of the kinetic factors that influences the complexity as well as the rate of the observed process. The stoichiometry of the homogeneous bimolecular redox reaction of HOIO disproportionation can be represented by the equation:

$$2HOIO \rightarrow IO_3^- + H^+ + HOI \quad (1)$$

Experimental determinations are relatively difficult since the measurements are hard to perform in the same way due to the high concentration of sulfuric acid in the preparation of HOIO and very limited in terms of the observed results. Calculated kinetic parameters, based on experimental measurements such as reaction rate and the activation energy of this reaction, have been determined in relatively precise and accurate manner, whereas their published values significantly differ (Noszticzius et al., 1983; Lengyel et al., 1996).

In addition to experimental, theoretical and numerical research are of great importance for complete understanding of the process. Particularly important is the knowledge of the ionic species concentrations that are formed at the beginning of the disproportionation reaction and remain unchanged during their evolution. Our previously published studies decribe the application of numerical and theoretical methods for their determination (Markovic et al., 2015).

The aim of this paper is to examine the HOIO disproportionation reaction depending on the system temperature using experimental and theoretical methods. Kinetic parameters, such as rate constants and activation energy, were determined experimentally at defined acidity in aqueous sulfuric acid solution, as well as at different system temperatures. Numerical simulation of the experimentally obtained results was performed using the Hindmarsh version of the Gear's integrator (Markovic et al., 2002). Under isothermal conditions, the concentrations of the relevant species H^+, H_2OI^+ and IO_3^- were determined theoretically based on their numerical evaluation.

* Corresponding author: smiljana.markovic@pr.ac.rs

EXPERIMENTAL

The experiments are performed in a similar manner as described in our previously published papers (Markovic et al., 2002; Markovic & Petrovic, 2016). The kinetics of the iodous acid disproportionation reaction was indirectly monitored by UV-Vis spectrophotometric method in 10 mm quartz cuvettes. The absorption changes of the resulting mixture were monitored at 274 nm (absorption maximum I_2, ε=183m^{2}mol^{-1}). Fresh and thermostated solutions prepared immediately before the experiments were used for experimental determinations. Double-distilled water and analytical pure reagents (Merck, Emd Chemicals, Inc. Gibbstown, NJ) were used for the preparation of stock solutions.

Dissolution of I_2 in excess of KIO_3 (in a ratio of 1: 5) in concentrated sulfuric acid (96%) gives a mixture containing I^+ and I^{3+} ionic species (Noszticzius et al., 1983). The stoichiometry of the overall complex reaction can be described as:

$$I_2 + 3IO_3^- + 8H^+ \rightarrow 5IO^+ + 4H_2O \quad (2)$$

Reactions were performed in iodate excess in order to prevent I^+ formation. Namely, a balance mixture containing I^+, I^{3+}, and I^{5+} ions is formed in an acidic media, where their concentration is controlled by the initial ratio of concentrations of I_2 and IO_3^-. The ionic species is added in the form of liquid iodosyl sulfate $(IO)_2SO_4$ into 50 cm^3 solution of sulfuric acid concentration of 0.125 mol/dm^3. Then, the iodosyl ion in the aqueous solution decomposes rapidly forming I^{3+} which is presented in the form of iodous acid:

$$IO^+ + H_2O \rightarrow H_2IO_2^+ \rightarrow H^+ + HOIO \quad (3)$$

All measurements are performed in several independent series. Each new series is preceded by experiments that reproduce some of the results of previous series. The study of the disproportionation reaction was performed under conditions of a closed isothermal well-stirred reactor, where the temperature of the reaction mixture was maintained constant, with an accuracy of ± 0.2 K. The solutions were kept in closed dark quartz vessels and the experiments were performed in semi-darkness without direct overhead lighting.

RESULTS AND DISCUSSION

The experimental results are shown in Table 1. The estimated disproportionation reaction rate constants were determined at 285, 291, 298 and 303 K with constant solution acidity of 0.125 mol/dm^3. The light absorbance is caused only by I_2 molecule absorption (Awtrey, & Connik 1951).

To determine the reaction rate constants, the experimental and numerical methods were combined in the manner shown earlier (Markovic et al., 2002). Furthermore, a previously accepted mechanism model was used, which was described in details in our previously published papers (Markovic & Petrovic, 2016). The overall stoichiometry of the disproportionation reaction can be represented as:

$$5HOIO \xrightarrow{k} I_2 + 3IO_3^- + H_2O + 3H^+ \quad (4)$$

Due to the complexity of the system, only the I_2 generated during the reaction can be followed continuously. For the given experimental conditions, the obtained rate low for the overall disproportionation process can be presented as:

$$d[HOIO]/dt = k[HOIO]^2 \quad (5)$$

where k is the rate constant of this process.

The complex reaction was examined in the concentration range from 3.23x10^{-4} to 7.10x10^{-4} mol/dm^3 for IO_3^-, while for HOIO values the concentrations were ranging from 1.40x10^{-4} to 1.80x10^{-4} mol/dm^3.

It can be noticed that within the analyzed concentration interval, the calculated values of the rate constants differ at different temperatures (Table 1, Fig. 1. S in the Supporting Information).

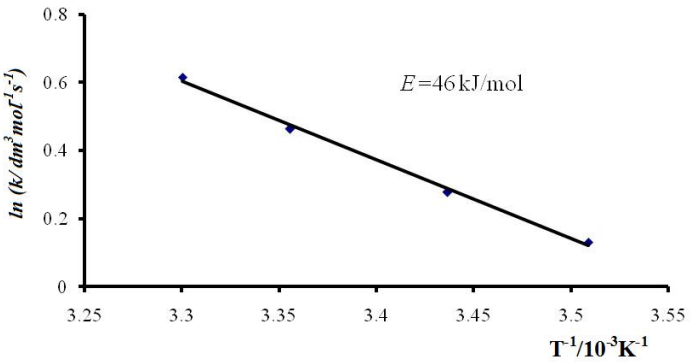

Figure 1. Dependence of ln k on 1/T.

Their values increase with increasing temperature and obtained values are about 1.6 times lower than in the case when the concentration of Hg^{2+} was in excess by 0.18 mol/ dm^3 (Markovic et al., 2002). The values of the rate constants are of the same order of magnitude (when the concentration of Hg^{2+} was in excess) and they are approximately 16 times lower than those given in the literature (Lengyel et al., 1996).

The amount of Hg^{2+} had no effect on the reaction rate constants of the process in the examined solutions, acidified with sulfuric acid; although we have prediced there would be an effect.

The influence of temperature and acidity as well as the very narrow limits of the feasible experimental conditions are probably main reasons for obtaining these diverse rate constant values. For the given experimental conditions, the average value of the activation energy was determined graphically as the slope of straight line from the dependence lnk = f(1/T), which represents the linear form of the Arrhenius equation, and is E_a = 46 kJ / mol. The dependence lnk = f(1/T), was plotted in Fig 1.

Table 1. HOIO disproportionation rate constants calculated at different temperatures obtained by measuring the increase in the absorption of I_2 molecular species at 274 nm.

T *K*	*[HOIO]* $moldm^{-3}\ x10^4$	$[IO_3^-]$ $moldm^{-3}\ x10^4$	$[H^+]$ $moldm^{-3}\ x10^4$	*k* $dm^3mol^{-1}s^{-1}$	k_{av} $dm^3mol^{-1}s^{-1}$
285	1.80	3.23	0.125	1.16	
	1.74	4.80		1.14	
	1.70	5.10		1.20	1.14±0.08
	1.54	6.00		1.12	
	1.40	7.10		1.10	
291	1.80	3.23	0.125	1.40	
	1.74	3.23		1.38	
	1.70	4.80		1.35	1.32±0.10
	1.50	5.10		1.23	
	1.40	6.00		1.26	
298	1.80	3.23	0.125	1.80	
	1.70	3.23		1.70	
	1.54	5.10		1.60	1.59±0.07
	1.40	6.00		1.40	
	1.40	7.10		1.48	
303	1.80	5.10	0.125	2.02	
	1.78	4.80		1.98	
	1.74	4.80		1.80	1.85±0.10
	1.10	6.00		1.75	
	1.20	3.23		1.68	

Table 2. Equilibrium concentrations ($moldm^{-3}$) of relevant ionic species estimated numerically, $[H_2SO_4]_{tot} = 0.125 moldm^{-3}$, $[SO_4^{2-}]_{tot} = 0.0104\ moldm^{-3}$, $[HSO_4^-]_{tot} = 0.083\ moldm^{-3}$ for various values of $[HOIO]_{tot}$.

$[KIO_3]$ $moldm^{-3}\ x10^4$	3.23	4.80	5.10	6.00	7.10
$[IO_3^-]$ $(moldm^{-3})$	0.066	0.080	0.083	0.090	0.101
	0.067	0.082	0.086	0.094	0.105
	0.071	0.086	0.090	0.098	0.110
	0.074	0.092	0.096	0.105	0.116
	0.078	0.098	0.100	0.112	0.124
$[H_2OI^+]$ $(moldm^{-3})$	0.052	0.077	0.082	0.096	0.114
	0.055	0.080	0.085	0.100	0.115
	0.060	0.081	0.087	0.102	0.117
	0.062	0.090	0.096	0.113	0.129
	0.066	0.095	0.106	0.124	0.142
$[H^+]$ $(moldm^{-3})$	0.175	0.192	0.195	0.205	0.216
	0.187	0.202	0.210	0.215	0.228
	0.191	0.215	0.220	0.230	0.248
	0.195	0.225	0.228	0.240	0.266
	0.205	0.230	0.239	0.255	0.274

The obtained value is lower in comparison to the previously published (Markovic et al., 2002) and confirms the presence of catalytic influences in the disproportionation process, what is in agreement with previous observations (Markovic & Cekerevac 2009; Markovic & Rakicevic 2006; Hegedűs et al., 2001; Markovic & Petrovic, 2010).

During the disproportionation proces, the concentrations of catalytic and relevant species of H^+, H_2OI^+ and IO_3^- , formed at the beginning of the reaction, are relatively high and under negligible changes. This is completely different from the behavior I_2, and other species, such as the intermediates I^-, HIO, HOIO, and others (Lengyel et al., 1996). Under our isothermal conditions in the quasi-stationary state of *pseudo*-equilibrium concentrations of these relevant species, disproportionation reactions were determined during equilibrium dissociation reactions for strong acid sulfuric acid, using previously described procedure (Markovic et al.,2015) and based on the equations:

$$\left[SO_4^{2-}\right]_{tot} = \left[SO_4^{2-}\right]\left(1+\beta_{a2}\left[H^+\right]+\beta_{a1}\left[H^+\right]^2\right) \qquad (6)$$

$$\left[IO_3^-\right]_{tot} = \left[IO_3^-\right]\left(1+\beta_{a3}\left[H^+\right]^3/\left[HIO_2\right]\right)+2\left[HIO_2\right] \quad (7)$$

$$\left[H^+\right]_{tot} = \left[H^+\right]\left(1+2\beta_{a1}\left[SO_4^{2-}\right]+\beta_{a2}\left[SO_4^{2-}\right]\right)+ \\ +\beta_{a3}\left[H^+\right]^2+\left[IO_3^-\right] \quad (8)$$

where: $\beta_{a1}-\beta_{a3}$ are stability constants previously known or estimated.

The results are shown in Table 2, for acidity of 0.125 mol/dm^3 and temperature of 298 K. The calculated concentration values are constant if HOIO concentration varies between 1.40x10^{-4} to 1.80x10^{-4} mol/dm^3. Thereby, the pH value was in the range of 1.5 to 3. The concentrations SO_4^{2-}, and HSO_4^- are small enough to be neglected, so they were not taken into account in this consideration. These results indicate that for certain values of initial sulfuric acid concentration, the *pseudo*-equilibrium concentration of iodate IO_3^- and H^+ ions is a linear and monotonously increasing function of the initial concentrations of potassium iodate (Figures 2 and 3).

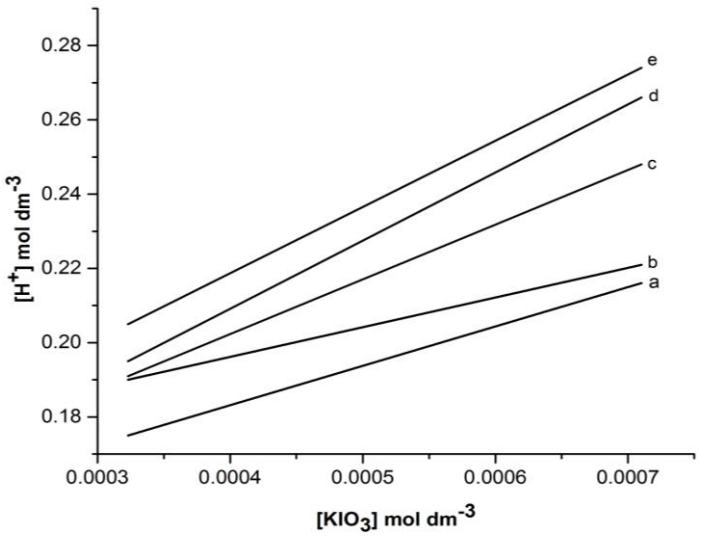

Figure 2. Equilibrium concentrations of [H^+] as a function of [KIO_3] for various values of $[HOIO]_{tot}$ at 298 K, a; $[HOIO]_{tot}$ = 1.8x10^{-4} moldm^{-3}, b; $[HOIO]_{tot}$ = 1.74 x10^{-4} moldm^{-3}, c; $[HOIO]_{tot}$ = 1.70 x10^{-4} moldm^{-3}, d; $[HOIO]_{tot}$ = 1.54 x10^{-4} moldm^{-3}, e; $[HOIO]_{tot}$ = 1.40 x10^{-4} moldm^{-3}.

The results of equilibrium concentrations at 298 K are presented here, while their trends are of a general character.

The resulting values of the observed concentrations of sulfuric and iodous acid, determined from the equilibrium dissociation reactions in the quasi-stationary state, are predominant and higher than of the protonated ion H_2OI^+ of hypoiodic acid.

Concentrations of other species in the system are relatively small under the given conditions which can be neglected. The influence of salt was not taken into consideration because there is no influence on the rate of the process since the neutral HOIO molecule is disproportionated.

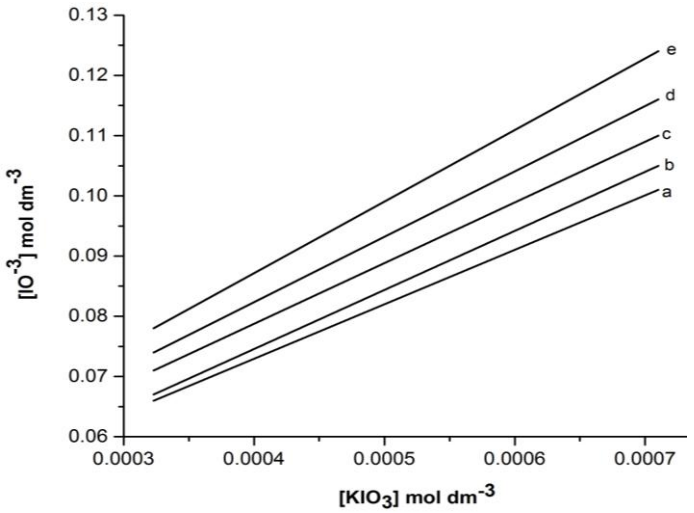

Figure 3. Equilibrium concentrations of [IO_3^-] as function of [KIO_3] for various values of $[HOIO]_{tot}$ at 298 K, a; $[HOIO]_{tot}$ = 1.8x10^{-4} moldm^{-3}, b; $[HOIO]_{tot}$ = 1.74 x10^{-4} moldm^{-3}, c; $[HOIO]_{tot}$ = 1.70 x10^{-4} moldm^{-3}, d; $[HOIO]_{tot}$ = 1.54 x10^{-4} moldm^{-3}, e; $[HOIO]_{tot}$ = 1.40 x10^{-4} moldm^{-3}.

On the base of the date obtained in the corresponding temperature interval thermodynamic parameters are calculated: $\Delta H = (-17.5 \pm 1)$ kJmol^{-1}, $\Delta S = (160 \pm 3)$ JK^{-1} mol^{-1}. These found values shows that overall reaction (4) for disproportionation HOIO is thermodynamically possible for given values of the initial concentration of reactants and the temperature in studied system.

CONCLUSION

The HOIO iodous acid disproportionation reaction and the effect of the acidity in solutions containing 0.125 mol/dm^3 sulfuric acid was analysed. Values of kinetic parameters, such as reaction rate constants and activation energy were determined based on a series of spectrophotometric measurements of absorption changes of I_2 molecular species at 274 nm, generated during the reaction. By changing concentrations from 3.23x10^{-4} to 7.10x10^{-4} mol/dm^3 for IO_3^-; and from 1.40x10^{-4} to 1.80x10^{-4} mol/dm^3 for HOIO, the influence of temperature (in the range of 285-303 K) on the kinetics of this complex reaction under stationary conditions was examined. For the selected temperature range, the disproportionation average rate constants ranged from 1.14 ± 0.08 dm^{3}mol^{-1}s^{-1} to 1.85 ± 0.10 dm^{3}mol^{-1}s^{-1}, respectively. According to the obtained results, increase of the reaction rate with increasing temperature was observed for different values of the iodous acid and iodate concentration. The average value of activation energy is determined graphically from temperature dependence of the rate constants, equals of E_a = 46 kJ/mol. The values for enthalpy and entropy activation were determined.

Under the examined isothermal conditions, the *pseudo*-equilibrium values of the concentrations of the relevant ionic species H^+, H_2OI^+ i IO_3^- were determined from the equilibrium dissociation reactions for sulfuric acid and the iodous acid disproportionation reaction in the quasi-stationary state. Their values are predominant and higher than the concentration of the protonated H_2OI^+ ion under given conditions.

ACKNOWLEDGEMENT

This work was funded in part by the Ministry of Education, Science and Technological Development of the Republic of Serbia (Project No. III 43007).

REFERENCES

Awtrey, A. D. & Connik, R. E. J. 1951. The Absorption Spectra of I_2, I_3^-, I^-, IO_3^-, $S_4O_6^=$ and $S_2O_3^=$. Heat of the Reaction $I_3^- = I_2 + I^-$. Journal of the American Chemical Society, 73(4) pp. 1842-1843.

De Souza G. L. C. & Brown A. 2014. Probing ground and low-lying excited states for HIO_2 isomers, J Chem Phys, 141(23), pp.234-303. https://doi.org/10.1063/1.4903789

Hegedűs, L., Wittmann, M., Noszticzius, Z., Yan, S., Sirimungkala, A., Försterling, H. & Field, R. J. 2001. HPLC analysis of complete BZ systems. Evolution of the chemical composition in cerium and ferroin catalysed batch oscillators: experiments and model calculations. Faraday Discussions, (120)21-38, pp. 85-104. https://doi.org/10.1039/B103432B

Jimenez J. L., Cocker D. R., Bahreini R., Zhuang H., Varutbangkul V., Flagan R. C., Seinfeld J. H., O'Dowd C., & Hoffmann T. 2003. New particle formation from photooxidation of diiodomethane (CH_2I_2). J. Geophys Res–Atmos, 108(D10), pp.4318. https://doi.org/10.1029/2002JD002452

Lengyel, I., Li, J., Kustin, K. & Epstein I. R. 1996. Rate Constants for Reactions between Iodine- and Chlorine-Containing Species: A Detailed Mechanism of the Chlorine Dioxide/Chlorite-Iodide Reaction †. Journal of the American Chemical Society, 118(15), pp. 3708-3719.

Mäkelä J. M., Hoffmann T., Holzke C., Väkevä M., Suni T., Mattila T., Aalto P. P., Tapper U., Kaupinen E. & O'Dowd C. 2002. Biogenic iodine emissions and identification of end-products in coastal ultrafine particles during nucleation bursts. J. Geophys. Res, 107(19), pp. 8110. https://doi.org/10.1029/2001JD000580

Marković, S., Rakićević, N. & Mišljenović, Đ. 2002. The temperature dependence of the disproportionation reaction of iodous acid in aqueous sulfuric acid solutions. Journal of the Serbian Chemical Society, 67(5), pp. 347-351. DOI: 10298/JSCO205347M

Marković, S. & Rakićević, N. 2006. Determination of the rate of iodous acid disproportionation in aqueous sulfuric acid solution. Reaction Kinetics and Catalysis Letters, 89(1) pp. 3-8. DOI: 10.107/S114-0.06-0.080-9

Marković, S. & Čekerevac, M. 2009. The rate of the disproportionation reaction of iodous acid at different acidity values in aqueous sulfuric acid solution. Reaction Kinetics and Catalysis Letters, 97(1), pp. 13-18. DOI: 10.107/S114-0.09-0.03-7

Marković, S. & Petrović, B. 2010. Kinetics of the disproportionation reaction of HIO_2 in acidic aqueous solutions. International Journal of Chemical Kinetics, 42(11) pp. 687-691. DOI: 10.102/kin20516

Marković, S., Karkalic, R. & Petrović, B. 2015. Disproportionation reaction of iodous acid, HOIO. Determination of the concentrations of the relevant ionic species H^+, H_2OI^+, and IO_3^-. Research on Chemical Intermediates, 41(3) pp. 1293-1300. DOI: 10.107/s164-0.13-1273-2.

Marković, S. & B. Petrović, B. 2016. Kinetics study of the disproportionation of the iodous acid inaqueous sulfuric acid solution, University thought, Publication in Natural Sciences, 6, (1), pp. 27-31. DOI: 10.5937/univtho6-10474

Noszticzius, Z., Noszticzius, E. & Schelly, Z. A. 1983. Use of ion selective electrodes for monitoring oscillating reactions, 2. Potential response of bromide-iodide selective electrodes in slow corrosive processes, Disproportionation of bromous and iodous acids. A Lotka-Voltera model for the halate oscil. Journal of Physical Chemistry, 87(3), pp. 510-524.

O'Dowd, C. D., Jimenez, J. L., Bahreini, R., Flagan, R. C., Seinfeld, J. H., Hämeri K., Pirjola L., Kulmala M., Jennings S. G. & Hoffmann T. 2002. Marine aerosol formation from biogenic iodine emissions. Nature 417, pp. 632–636. https://doi.org/10.1038/nature00775

Urbansky, E. T., Cooper B. T. & Margerum, D. W. 1997. Disproportionation Kinetics of Hypoiodous Acid As Catalyzed and Suppressed by Acetic Acid-Acetate Buffer, 36(7) pp. 1338-1344. https://doi.org/10.1021/ic960745z

Bulletin of Natural Sciences Research
Vol. 11, No. 2, 2021, pp. 25-28.

DOI: https://doi.org/10.5937/bnsr11-31292
Original Scientific Paper

LIGHT CAPTURING WITHIN THE DEFECT LOCATED IN LINEAR ONE-DIMENSIONAL PHOTONIC LATTICE

SLAVICA JOVANOVIĆ[1], MARIJA STOJANOVIĆ KRASIĆ[2]

[1]Faculty of Sciences and Mathematics, University of Priština in Kosovska Mitrovica, Kosovska Mitrovica, Serbia
[2]Faculty of Technology, University of Niš, Leskovac, Serbia

ABSTRACT

Numerically investigated the light beam propagation through one-dimensional photonic lattice possessing one linear defect. It is shown how capturing of light depends on lattice characteristics as well as the width and wavelength of input light beam. Results may be useful for all-optical control of transmission of waves in interferometry.

Keywords: Photonic lattices, Linear defect, Trapping efficiency, Optical control.

INTRODUCTION

Wave propagation in periodic optical lattices has been intensively studied in the last years. Photonic lattices (PL) are periodic structures that are widely used for light manipulation in photonic devices (Song et al., 2003). Their periodic structures enable the study as discrete diffraction (Eisenberg et al., 2000) the existence of Bloch oscillations (Peschel et al., 1998) discrete and gap solitons (Christodoulides et al., 2003; Neshev et al., 2007; Garanovich et al., 2012). Localized modes can be formed inside the lattice and are influenced by the very geometry of photonic systems, such as modulated lattices (Cao et al., 2012) and flat-band lattices (Vicencio et al., 2015; Beličev et al., 2015). The periodicity enables formation of zonal structure. The zonal structure consists of permitted and forbidden zones which can allow or stop light beam propagation. The zonal structure can be changed by introducing defect into the lattice (Yablonovitch, 1993; Meade et al., 1993). Control of light propagation in one-dimensional (1D) photonic crystals is possible by changes system parameters, such as refractive index, lattice period and the width of defect (Suntsov et al., 2006; Matias et al., 2003; Kuzmanović, 2016; Stojanović Krasić et al., 2017). The defects disrupt translational symmetry and enables the formation of localized defect modes (Gupta et al., 1997, Tsai et al., 1998). Defects in PL may stop light (Goodman et al., 2002), trap or deflect the incident beam (Molina et al., 2006). Can be used for all-optical switching and routing (Wang et al.; 2009, Ye et al., 2008). Defects be formed by changing the value of refractive index in certain WG or by changing the width of the WG or the distance between WGs (Meier et al., 2005, Morandotti et al., 2003). Lattice defects increase the complexity of the zonal structure by creating defect levels within the gaps (Beličev et al., 2010; Fedele et al., 2005; Molina et al., 2008).

The propagation of waves in periodic systems with linear and nonlinear defects were investigated (Mak et al., 2003; Molina et al., 2006) and the scattering of linear and nonlinear waves in series with a PT-symmetric defect (Dimitriev et al., 2011). Structural defect significantly influences the propagation of light beams in the vicinity of lattices compound and enables the existence of various localized components.

In this work, we numerically analyze how light capturing is affected by lattice parameters and by light characteristics such as wavelength and full width at half maximum.

THEORETICAL PART

We analyze the linear one-dimensional PL which contains a linear defect (LD) embedded (Figure 1).

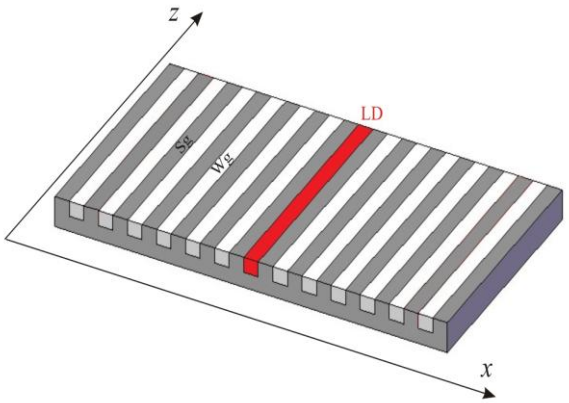

Figure 1. Schematic representation of the system. red line shows the position of the linear defect.

The light propagation through PL consisting of the linear waveguide array with embedded single linear waveguide. Mathematically, the model can be described with the paraxial time-independent Helmholtz equation (Kuzmanović et al., 2015):

$$i\frac{\partial E}{\partial z}+\frac{1}{2k_0n_0}\frac{\partial^2 E}{\partial x^2}+k_0n_0n(x)E=0 \qquad (1)$$

* Corresponding author: slavica.jovanovic@pr.ac.rs

where z is the propagation coordinate, $E(x,z)$ is the component of the light electric field in the z-direction, $k_0 = 2\pi/\lambda$ is the wave number, n_0 is the refractive index of the substrate, and λ is the wavelength of light. The lattice is prepared along the transverse x direction and there are 49 WGs in each lattice. Functional dependence of the refractive index on system parameters (Kuzmanović et al., 2016) given by in the form:

$$n_l(x) = \Delta n \left(\sum_{j=1}^{k-1} G(w_g, s, x) + G_k(w_{gk}, s_k, x) + \sum_{j=k+1}^{m} G(w_g, s, x) \right) \quad (2)$$

where k is the position of the LD which is arbitrary placed in the lattice, m is the number of WGs in lattice Δn is the lattice potential depth. Parameters w_g mark the width within lattice. The parameter w_{gk} represents the width of the LD, while parameters s represents the spacing between WGs in the lattices. Functions $G(w_g, s, x)$ represent Gaussians corresponding to the WGs of the lattice, whereas function $G_k(w_{gk}, s_g, x)$ corresponds to the LD. Lattice potential depth is 0.011.

The explicit form of Gaussians is:

$$G_n(x, w_g, s) = \sqrt{\frac{4\ln 2}{\pi w_g^2}} \exp\left(-\left(\frac{x - ns}{w_g} \right)^2 4\ln 2 \right) \quad (3)$$

that models the waveguides refractive index profile (Kuzmanović et al., 2015).

The position of the center of the nth component Gaussian is marked ns, and it is shifted from the middle of the waveguide along the x axis. The respective width w_g represents the full width at half maximum.

Introducing dimensionless variables $\xi = k_0 x$ and $\eta = k_0 z$, the equation (1) obtained the following dimensionless form:

$$i\frac{\partial E}{\partial n} + \frac{1}{2n_0}\frac{\partial^2 E}{\partial \xi^2} + n_0 n(\xi) E = 0 \quad (4)$$

The light propagation across the lattice is initiated by the Gaussian light beam with wavelength λ = 450 nm and λ = 550 nm with the FWHM as a variable parameter. In the following, we use either Gaussian light beam with the FWHM = 1,5 μm, 2 μm, 3,5 μm, 4 μm and 6 μm. The light propagation is simulated numerically by the split-step Fourier method (Fisher & Bischel 1973).

NUMERICAL RESULTS

The aim of the numerical results is to compare how lattice parameters, as well as beam characteristics, affect light capturing at the 2 μm and 6 μm wide defect. The width of the LD is either 2 or 6 μm and further in the paper they will be marked as narrow and wide defect, respectively. The width of the WG within the lattice is variable parameter and we analyse $w_g = 3.5$ μm, 4 μm, 4.5 μm and 5 μm and the distance between neighboring WGs is $s_g = 3.5$ μm, 4 μm and 4.5 μm. LD is fixed in the middle of the lattice and its position does not change.

In general, the trapping efficiency in a lattice with a coupling defect depends on the wavelength of used light (please see Fig. 3 below) and the coupling strength of the defect compared to the rest of the lattice. Keeping the size of the defect and the wavelength of used light constant, the coupling strength may be changed either by changing the parameters of the uniform lattice (please see Figs. 2a and 2b) or by varying the FWHM of the input beam (please see Fig. 2, 3).

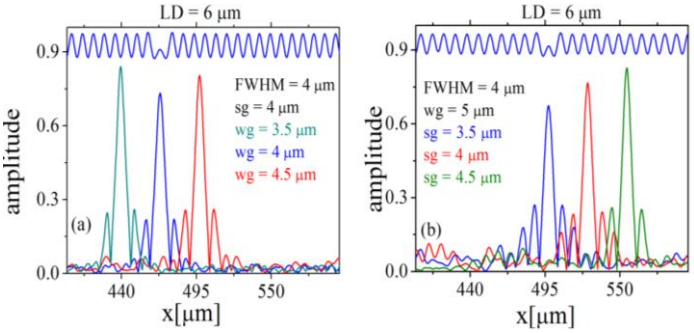

Figure 2. Amplitude profiles of the output light beams. Light (FWHM = 4 μm) is captured at the 6 μm wide LD in the lattice: a) The separation between waveguides is constant, while their width is the changeable parameter: 3.5 μm - green, 4 μm - blue and 4.5 μm – red colour. b) The width of the waveguides is constant and the separation between them is the varying parameter: 3.5 μm – blue, 4 μm – red, 4.5 μm – green colour. The potential of the lattice is schematically represented within the plots – blue curve in Figs. 2. a, b.

Light capturing at the 6 μm wide LD within the lattice, where the distance between the waveguides is constant (s_g) and where the width of the waveguides (w_g) is the varying parameter, is shown in Fig. 2a. Because of the different periods of the lattices, caused by diverse widths of the waveguides (3 μm, 4 μm, 4.5 μm), the positions of the LDs are shifted along the x – axis (see the positions of the green, blue and red curve). The potential of one of the lattices ($w_g = 4$ μm) is schematically represented in Fig. 2, 3, for the better readability. One may see that the different widths of the waveguides influence the amplitudes of defect modes (green, blue and red curve).

Light capturing at the 6 μm wide LD within the lattices where the width of the waveguides is constant and where the separation between the waveguides is the changeable parameter, is presented in Fig. 2b. It is obvious that different separations

between the waveguides influence the trapping efficiency of the observed defect modes (see blue, red and green curve in the Fig. 2b).

Capturing of light at the 6 μm wide LD for two different wavelengths is presented in Fig. 3. There is a slightly difference between the amplitudes' heights when the wavelength of the used light is 450 nm or 550 nm (see red curve and red curve in Fig. 3).

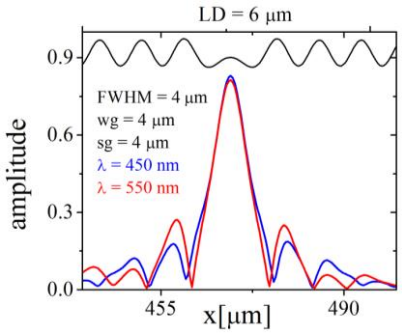

Figure 3. Amplitude profiles of the output light beams. Light (FWHM = 4 μm) is captured at the 6 μm wide LD in the lattice with $w_g = 4\,\mu m$ and $s_g = 4\,\mu m$. The blue curve denotes a light beam with the wavelength of 450 nm, while the red one marks the light beam with the wavelength of 550 nm. The potential of the lattice is schematically represented within the plots – black curve in Fig. 3.

In Fig. 4a and Fig. 4b it can be seen that the input of 4 μm gives the best capturing effect at the 6 μm wide LD (see red curve in Fig. 4a). In Fig. 4b, it can be seen that at the 2 μm wide LD the narrower input beam (2 μm FWHM) enables slightly better capturing (see – green colour in Fig. 4b).

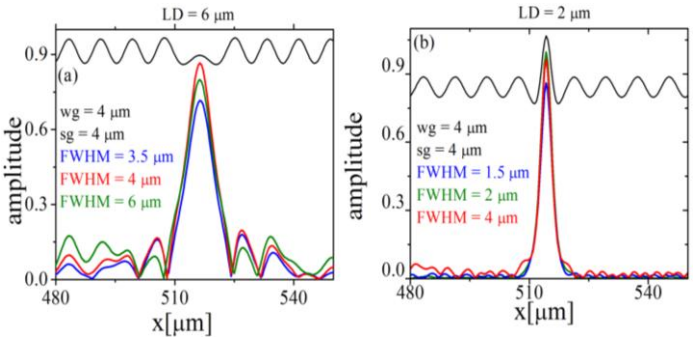

Figure 4. Amplitude profiles of the output light beams. Light is launched in the lattice where $w_g = 4\,\mu m$ and $s_g = 4\,\mu m$, at the: a) 6 μm wide LD. FWHM of the input beam is: 3.5 μm – blue, 4 μm – red, 6 μm – green. b) 2 μm wide LD. FWHM of the input beam is: 1.5 μm – blue, 2 μm – green, 4 μm – red. The potential of the lattice is schematically represented within the plots – black curve in Fig. 4.

CONCLUSION

We have numerically explored how LDs of different widths affect light beam propagation through a PL system with a LD. The chosen set of system parameters, the narrower LD is more efficient in light entrapment. The difference of light capturing is analyzed through varying the system parameters, waveguide width and separation between waveguides, and also by changing the characteristics of the light beam such as FWHM and waveguide.

ACKNOWLEGMENTS

The authors acknowledge support from project the financed by the Faculty of Sciences and Mathematics, Kosovska Mitrovica (Project No. ИЈ-0201) and program for financing scientific research work (No. 451-03-9/2021-14/200133).

REFERENCES

Beličev, P., Ilić, I., Stepić, M., Maluckov, A., Tan, Y. & Chen, F. 2010. Observation of linear and nonlinear strongly localized modes at phase-slip defects in one-dimensional photonic lattices. Opt. Letters, 35, pp. 3099-3101. https://doi.org/10.1364/OL.35.003099

Beličev, P. P., Gligorić, G., Radosavljević, A., Maluckov, A., Stepić, M., Vicencio, R. A. & Johansson, M. 2015. Localized modes in nonlinear binary kagome ribbons. Phys. Rev. E., 92, pp. 052916. https://doi.org/10.1103/PhysRevE.92.052916

Cao, Z., Qi, X., Feng X., Ren, Z., Zhang, G. & Bai, J. 2012. Light controlling in transverse separation modulated photonic lattices. Opt. Exp., 20, pp. 19119-19124. https://doi.org/10.1364/OE.20.019119

Christodoulides, D. N., Lederer, F. & Silberberg, Y. 2003. Discretizing light behaviour in linear and nonlinear waveguide lattices. Nature, 424, pp. 817–823. http://dx.doi.org/10.1038/nature01936

Dmitriev, S. V., Suchkov, S. V., Sukhorukov, A. A. & Kivshar, Y. S. 2011. Scattering of linear and nonlinear waves in a waveguide array with a PT-symmetric defect. Phys. Rev. A., 84, pp. 013833. https://doi.org/10.1103/PhysRevA.84.013833

Eisenberg, H. S, Silberberg, Y, Morandotti, R. & Aitchison, J. S. 2000. Diffraction Management. Phys. Rev. Lett., 85, pp. 1863. DOI: https://doi.org/10.1103/PhysRevLett.85.1863

Fedele, F., Yang, J. K., & Chen, Z. G. 2005. Defect modes in one-dimensional photonic lattices. Opt. Letters, 30, pp. 1506-1508. https://doi.org/10.1364/OL.30.001506

Fisher, R. A., & Bischel, W. K. 1973. The role of linear dispersion in plane-wave self-phase modulation. Applied Physics Letters, 23, pp. 661. https://doi.org/10.1063/1.1654782

Garanovich, I. L., Longhi, S., Sukhorukov, A. A. & Kivshar, Y. S. 2012. Light propagation and localization in modulated photonic lattices and waveguides. Phys. Rep., 518, pp. 1-79. https://doi.org/10.1016/j.physrep.2012.03.005

Goodman, R. H., Slusher, R. E. & Weinstein, M. I. 2002. Stopping light on a defect. J. Opt. Soc. Am. B., 19, pp. 1635-1652. https://doi.org/10.1364/JOSAB.19.002737

Gupta, B. C. & Kundu, K. 1997. Formation of stationary localized states due to nonlinear impurities using the discrete nonlinear Schrödinger equation. Phys. Rev. B., 55, pp. 894-905. https://doi.org/10.1103/PhysRevB.55.894

Kuzmanović, J. S. 2015. Kontrola formiranja i prostiranja lokalizovanih struktura u fotonskim rešetkama s defektima. Niš: PMF Niš.

Kuzmanović, S., Stojanović Krasić, M., Milović, D., Radosavljević, A., Gligorić, G., Maluckov, A. & Stepić, M. 2015. Defect induced wave-packet dynamics in linear one-dimensional photonic lattices. Phys. Scripta, 90, pp. 025505. https://doi.org/10.1088/0031-8949/90/2/025505

Kuzmanović, S., Stojanović Krasić, M., Mančić, A., Drljača, B. & Stepić, M. 2016. The influence of nonlinear and linear defects on the light propagation through linear one-dimensional photonic lattice. University Thought, 6, pp. 61-66. DOI: 10.5937/univtho6-12670

Mak, W. C. K., Malomed, B. A., & Chu, P. L. 2003. Interaction of a soliton with a local defect in a fiber Bragg grating. J. Opt. Soc. Am. B., 20, pp. 725-735. https://doi.org/10.1364/JOSAB.20.000725

Matias, I. R., Villar, I. D., Arregui, F. J. & Claus, R. O. 2003. Development of an optical refractometer by analysis of one-dimensional photonic bandgap structures with defects. Opt. Lett., 28, pp. 1099–1101. DOI: 10.1364/ol.28.001099

Meade, R. D., Rappe, A. M., Brommer, K. D., Joannopoulos, J. D. & Alerhand, O. L. 1993. Accurate theoretical analysis of photonic band-gap materials. Phys. Rev. B., 48, pp. 8434-8437. https://doi.org/10.1103/PhysRevB.48.8434

Meier, J., Stegeman, I. G., Christodoulides, D. N., Silberberg, Y., Morandotti, R., Yang, H., Salamo, G., Sorel, M. & Aitchison J. S. 2005. Beam interactions with a blocker soliton in one-dimensional arrays. Opt. Letters, 30, pp. 1027-1029. https://doi.org/10.1364/OL.30.001027

Molina, M. I. & Kivshar, Yu. S. 2008. Nonlinear localized modes at phase-slip defects in waveguide arrays. Opt. Letters, 33, pp. 917-919. https://doi.org/10.1364/OL.33.000917

Molina, L. M. & Vicencio, R. A. 2006. Trapping of discrete solitons by defects in nonlinear waveguide arrays. Opt. Lett., 31, pp. 966-968. https://doi.org/10.1364/OL.31.000966

Morandotti, R., Eisenberg, H. S., Mandelik, D., Silberberg, Y., Modotto, D., Sorel, D., Stanley, C. R. & Aitchison, J. S. 2003. Interactions of discrete solitons with structural defects. Opt. Letters., vol. 28, pp. 834-836. https://doi.org/10.1364/OL.28.000834

Neshev, D. N., Sukhorukov, A. A., Krolikowski, W. & Kivshar, Y. S. 2007. Nonlinear optics and light localization in periodic photonic lattices. J. Nonlinear Opt. Phys. & Mater., 16, pp. 1-25. https://doi.org/10.1142/S0218863507003548

Peschel, U., Pertsch, T. & Lederer, F. 1998. Optical Bloch oscillations in waveguide arrays. Optics Letters, 23, pp. 1701-1703. https://doi.org/10.1364/OL.23.001701

Vicencio, R. A., Cantillano, C., Inostroza, L. M., Real, B., Cortez C. M., Weimann, S., Szameit, A. & Molina, M. 2015. Observation of Localized States in Lieb Photonic Lattices. Phys. Rev. Lett., 114, pp. 245503. https://doi.org/10.1103/PhysRevLett.114.245503

Song, B. S., Noda, S. & Asano, T. 2003. Photonic devices based on in-plane hetero photonic crystals. Science, 300, pp. 1537. DOI: 10.1126/science.1083066

Suntsov, S., Makris, K. G., Christodoulides, D. N., Stegeman, G. I., Haché, A., Morandotti, R., Yang, H., Salamo, G. & Sorel, M. 2006. Observation of discrete surface solitons. Phys. Rev. Lett., 96, pp. 063901. https://doi.org/10.1103/PhysRevLett.96.063901

Stojanović Krasić, M., Mančić, A., Kuzmanović, S., Veljković Đorić, S. & Stepić, M. 2017. Linear and interface defects in composite linear photonic lattice. Optics Communications, 394, pp. 6-13. DOI: 10.1016/j.optcom.2017.02.021

Tsai, Y. C. K., Shung, W. K. & Gou, S. C. 1998. Impurity modes in one-dimensional photonic crystals-analytic approach. J. Mod. Opt., 45, pp. 2147-2157. https://doi.org/10.1080/09500349808231751

Wang, X. & Chen, Z. 2009. Beam control and multi-color routing with spatial photonic defect modes. Opt. Exp., 17, pp. 16927-16932. DOI: 10.1364/OE.17.016927

Yablonovitch, E. 1993. Photonic band-gap structures. J. Opt. Soc. Am. B., 10, pp. 283-295. https://doi.org/10.1364/JOSAB.10.000283

Ye, F., Kartashov, Y. V., Vysloukh, V. A. & Torner, L. 2008. Nonlinear switching of low-index defect modes in photonic lattices. Phys. Rev. A., 78, pp. 013847. https://doi.org/10.1103/PhysRevA.78.013847

Bulletin of Natural Sciences Research
Vol. 11, No. 2, 2021, pp. 29-34.

DOI: https://doi.org/10.5937/bnsr11-28954
Original Scientific Paper

COMPARISON OF TRANSITION RATES WITH THE LG (0, 1)* SPIRAL-PHASE MODE FIELD DISTRIBUTION IN THE FRAME OF THREE IONIZATION THEORIES

TATJANA B. MILADINOVIĆ[1], NEBOJŠA S. DANILOVIĆ[2]

[1]Institute for Information Technologies Kragujevac, University of Kragujevac, Kragujevac, Serbia
[2]Faculty of Science, University of Kragujevac, Kragujevac, Serbia

ABSTRACT

We discussed the tunneling ionization of an Argon atom placed in a strong low-frequency field of Ti: Sapphire laser. The transition rate of the electron obtained with radial polarization LG (0, 1)* spiral-phase mode field distribution included are compared to the basic transition rate. All analyses are given in the frame of the three different ionization theories – Keldysh, PPT, and ADK. We demonstrated that the tunneling transition rate is sensitive to laser polarization and a set field distribution. As well as changes in the azimuthal angle as a parameter on which the given distribution depends.

Keywords: Tunneling ionization, Transition rate, Radially polarized LG (0, 1)* spiral-phase mode.

INTRODUCTION

The discovery of the laser in 1960 and the development of laser technology enabled research in several of areas. The study of the behavior of atomic and molecular systems that are exposed to the strong electromagnetic field of a high-power laser with a long or short pulse is one of those areas. First scientific papers dealing with these topics were written in the early 1970's (Keldysh, 1965; Voronov et al., 1966). During years the research was continued and the subject was expanded from the tunnel to multiphoton ionization (Xiong et al., 1991; Mainfray et al., 1991), barrier suppression (BSI) (Krainov et al., 1995) and above threshold ionization (ATI) (Eberly et al., 1988). These problems are still of interest to researchers, as evidenced by the latest work (Calvert et al., 2016; Lai et al., 2017; Shvetsov-Shilovski et al., 2019).

In order to explain the physical picture of laser interaction with an atom or molecule, it was necessary to give a theoretical basis. Over the years, several methods have created that can explain this physical phenomenon. Some of them are: numerically solving of the full-dimensional time-dependent Schrödinger equation (TDSE) (Parker et al., 1998; Parker et al., 2006), reduced-dimensional TDSE, strong field approximation (SFA) (Lappas et al., 1998; Liu et al., 1999), semiclassical method (Schafer et al., 1993; Corkum, 1993) and classical ensemble method (Panfili et al., 2001; Ho et al., 2006).

A semiclassical model, in which the atom is treated as a quantum object while the electromagnetic field is classical, will be used in this paper. The electron leaves the atom by tunneling while its trajectory in the field is classical. Landau and Lifshitz gave the basis and fundamental equations for the semiclassical model for the ionization of the hydrogen atom in the ground state, exposed to the influence of the electromagnetic field (Landau & Lifshitz, 1991). Among many later papers, Keldysh's work should be highlighted. Keldysh modified the given formula by including the influence of the electromagnetic field on the free electron (Keldysh, 1965). Also, he showed that multiphoton and tunnel ionization are two processes that are very similar in nature. As the boundary between these two processes, the Keldysh defined a parameter known as the Keldysh parameter $\gamma = \left(\omega\sqrt{2I_p}\right)/F$, where ω is the laser frequency, F the laser electric field strength and I_p, the ionization potential of the atom. When the parameter is $\gamma >> 1$, multiphoton ionization occurs, while in the case of $\gamma << 1$, tunnel ionization is the dominant process. Perelomov, Popov and Terent'ev (PPT) derived an equation that gives the tunneling transition rate of an arbitrary atom when changes in the external field can be neglected (Perelomov et al., 1966). Twenty years later, Ammosov, Delone and Krainov (ADK) extended the PPT theory to complex atoms and atomic ions (Ammosov et al., 1986).

Our research is focused on the influence of the shape of the laser pulse on the tunneling transition rate of the weakest bound electron of an Argon atom exposed to a strong laser field. The influence of Gaussian and Lorentzian beam shapes and different polarizations on ionization processes has been presented in numerous papers (Delone et al., 2000; Eichmann et al., 2009; Ooi et al., 2012; Ciappina et al., 2020). Since it has not been shown so far how Laguerre-Gaussian (LG) (0, 1)* beam with radial polarization affects this value, our intention was to investigate it. The radially-polarized pulse can be focused to a very small size (Dorn et al., 2003), which is ideal for electron acceleration and has an influence on its ionization. Also, we wanted to compare the behavior of the

*Coresponding author: tanja.miladinovic@gmail.com

transition rates calculated using Keldysh, PPT, and ADK theory for linear and LG $(0,1)^*$ spiral phase mode. Comparing these transition rates for elliptical and circular polarization are shown in the paper (Guo et al., 2019). Through the paper, atomic units were used $\left(m_e = |e| = \hbar = 1\right)$.

THEORETICAL PART

The tunneling ionization process of a quantum system (atom) is considered. The Theory of strong-field ionization, Keldysh Theory, gave the foundations for an understanding of this process. In the case of a ground state of a hydrogen atom, for large the field strength F and low the photon energy ω, the ionization rate (i.e., the probability of ionization per unit time) $w_{Keldysh}$ can be written (Keldysh, 1965):

$$w_{Keldysh} = \frac{\sqrt{3\pi Z F_{lin}}}{2^{7/4}} \times \exp\left[\frac{2Z^3}{3F_{lin}} \times \left(1 - \frac{1}{10}\frac{\gamma^2 Z^2}{2I_p}\right)\right] \quad (1)$$

Z is the charge of the ionized system, γ is the Keldysh parameter, while I_p is the ionization energy. The *lin* index in quantity F denotes that the observed laser field is linear polarized.

Perelomov, Popov and Terent'ev obtained an equation for transition rate, not only for ionization from the ground state but also from excited states. (Perelomov et al., 1966; Delone et al., 1998):

$$w_{PPT} = \sqrt{\frac{3n^3 F_{lin}}{\pi}} \frac{(2\ell+1)(\ell+|m|)! 2^{4n-2|m|-2} n^{-6n+3|m|}}{(n+1)!(n-\ell-1)!(|m|)!(\ell-|m|)!} \times \frac{\exp\left[-\frac{2}{3n^3 F_{lin}}\right]}{F_{lin}^{2n-|m|-1}} \quad (2)$$

where is n principal, ℓ orbital and m magnetic quantum number. Eq. (2) is applicable when the condition $F_{lin} < Z^3/16n^4$ is fulfilled (Bauer, 2006; Delone et al., 1999). Laser field strength is, smaller compared to the atomic field strengths for highly excited states of the hydrogen atom $\left(1/16n^4\right)$ even with the most intense lasers available today (Delone et al., 1999).

Amosov, Delone and Krainov included certain modifications in Eq. (2), so the formula could be used to calculate the transition rate in the case of complex atoms. For rough calculation of the factorials, Stirling's formula was used. Main quantum number n has been replaced by an effective quantum number $n* \equiv Z/\sqrt{2I_p}$ (Ammosov et al., 1986; Delone et al., 1998):

$$w_{ADK} = \sqrt{\frac{2n^{*3}F_{lin}}{\pi Z^3}} \frac{F_{lin}}{8\pi Z}\left(\frac{4\gamma\left(2I_p\right)^{3/2}}{\omega Z}\right)^{2n^*} \times \exp\left[-\frac{2}{3}\frac{2I_p\gamma}{\omega}\right] \quad (3)$$

Eqs. 1, 2, and 3 give the transition rates in a linearly polarized laser field. In this case, the relation between the intensity and the strength of the laser field is $F_{lin} : \sqrt{I}$ (in atomic units). The laser beam can have different profiles, for example, Gaussian and Lorentzian. Each of them has a specific field distribution $F_G = F\exp\left[-2\left(\rho/R\right)^2\right]$, (Tokarev et al., 2003) $F_L = F/\left(1+\left(\rho/R\right)^2\right)$ (David et al., 2005) where R is the diameter of Gaussian beam and has the smallest value for $z = 0$, while $\rho = R\sqrt{1+\left(\lambda z/\pi R^2\right)^2}$ is axial coordinate normal to the light ray (Zhang, 2010), λ is laser wavelength. The influence of these distributions on ionization processes has already been studied (Boutu et al., 2011; Ishkhanyan et al., 2015). We wanted to see how the quantities that describe these processes will behave when the field distribution is given by LG (0, 1)* spiral-phase mode (Machavariani et al., 2007):

$$F_{sp}\left(r,\phi\right) = F_0\sqrt{\rho_{sp}}e^{-\rho_{sp}/2}e^{\pm i\phi} \quad (4)$$

where r and ϕ are the cylindrical coordinates. Spiral is presented by polar equation $r\left(\phi\right) = ae^{k\phi}$ (a, k are parameters), $\rho_{sp} = 2r^2/R^2$ and sign ± depend on the chosen helicity. It is important to emphasize that LG (0, 1)* mode can appear with linear, circular or elliptical polarization (Machavariani et al., 2007; Shealya, et al., 2005).

For linear polarization, the electric field distribution of a spiral-phase LG (0, 1)* has the form:

$$\vec{F}_{lin,sp}\left(r,\phi\right) = F_{lin}\sqrt{\rho e}^{-\rho/2}e^{-i\phi}\left(\vec{e}_x + \vec{e}_y\right) \quad (5)$$

$\vec{e}_x$ and $\vec{e}_y$ presented the unite vectors along the x and y axis. In scalar form, Eq. (5) is given with the equation:

$$F_{lin,sp}\left(r,\phi\right) = F_{lin}\sqrt{pe}^{-\rho/2}\cos\phi\vec{e}_x\cdot\vec{e}_x \quad (6)$$

taking into account that is $\vec{e}_x\cdot\vec{e}_x = 1$.

In order to estimate the influence of LG (0, 1)* spiral-phase mode field's distribution with radial polarization on the transition rates given by Keldysh, PPT and ADK theories, we had to include Eq. (6) into Eqs. (1), (2) and (3).

NUMERICAL RESULTS

We discussed the tunnel ionization of the Argon atom exposed to the light of the Ti: Sapphire laser wavelength of $\lambda = 800nm$, while the photon energy in atomic units is $\omega = 0.5696$ a.u.. The binding energy of the first electron in the valence shell, of the Ar atom, in atomic units, is $I_p = 0.5791$ a.u. and the charge of this system will be $Z = 1$. The intensity of the laser field within the ionization process is observed in range $I = 10^{14} - 10^{17} W/cm^2$. The intensity of the laser field is given by I in W/cm^2, while the strength of this field with the linear polarization F_{lin} in V/cm, which is one of the ways to apply the semi-classical theory since other quantities are represented in the atomic system of units. Formally, the relationship between field strength and intensity can be represented by an expression $F_{lin} = 27.5\sqrt{I}$. In the case of LG (0, 1)* spiral-phase mode with radial polarization field strength is given by the Eq. (6).

Ti: Sapphire lasers can produce beams with different diameters, which can be the order of millimeters $(15-30)mm$ or micrometer $(3-60)\mu m$ (Dorn et al., 2003; Ahmmed et al. 2014). Radially polarized laser light produces a spot of smaller diameter. In our paper, we will assume that $R = 3\mu m\left(5.7\times10^4 \text{ in atomic units}\right)$. $r(\phi) = ae^{k\phi}$ is the cylindrical coordinate and is a function of parameters a and k, also on azimuthal angle Φ. Φ lies in a specific interval span of $360°$, such as $[-180°, +180°]$ or $[0°, +360°]$. $a = 0.57$ $\left(1.08\times10^4\right)$ when r is in μm, $k = \tan\theta$. Angle θ can take a value in the range of $[-90°, 90°]$ and defines spiral geometry (Ouyang, et al., 2015).

First, we focused on the comparison of the basic transition rate and the transition rate calculated with field distribution of LG (0, 1)* spiral-phase mode is included. The behavior of these rates as a function of laser intensity is observed.

In Figs. 1, 2 and 3 are shown obtained curves calculated using equations for Keldysh, PPT and ADK transition rates. In a given range of laser intensities, we can notice that the inclusion of the LG (0, 1)* spiral-phase field distribution leads to a decrease in the transition rate in all three observed cases. The analysis shown in Figures 1, 2, and 3 was done for azimuthal angle fixed to the value $\phi = 30°$ and laser intensity in range $I = 10^{14} - 10^{17} W/cm^2$. The values of the transition rates shown on the y-axis are given in arbitrary units.

At lower field intensities $I < 10^{15} W/cm^2$, the difference between the transition rates shown in Fig. 1 is imperceptible, the largest one is calculated for $I = 1.5\times10^{16} W/cm^2$, when $w_{Keldysh} = 0.272 a.u.$ and $w^{sp}_{Keldysh} = 0.008 a.u.$.

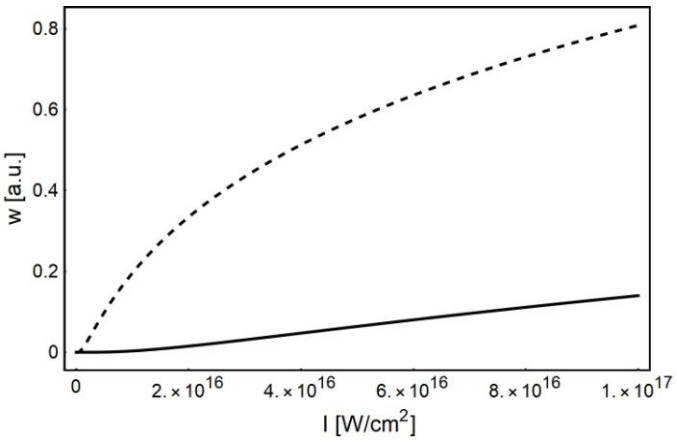

Figure 1. Keldysh tunneling transition rate as a function of laser intensity. $w_{Keldysh}$ (dashed line) and $w^{sp}_{Keldysh}$ (solid line) corresponds to the transition rate with linear polarization and with LG (0, 1)* spiral-phase mode, respectively.

We calculated that for $I = 10^{14} W/cm^2$, the difference between w_{PPT} and w^{sp}_{PPT} is negligible. With an increase in laser intensity, the difference becomes more noticeable. For $I = 1.75\times10^{16} W/cm^2, w^{sp}_{PPT}$ reaches only 15% of the value of w_{PPT} (Fig. 2.).

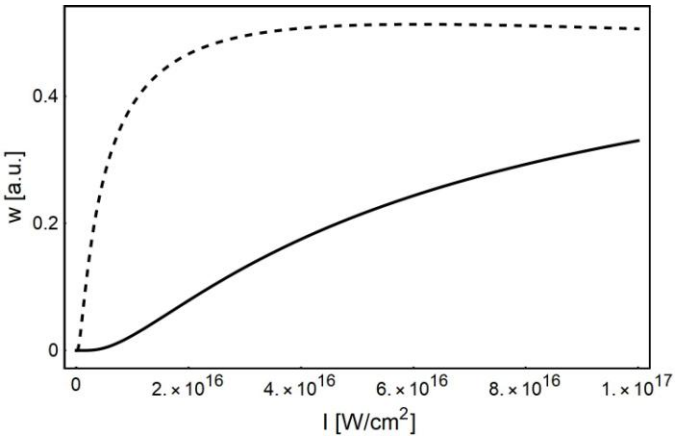

Figure 2. PPT tunneling transition rate as a function of laser intensity. w_{PPT} (dashed line) and w^{sp}_{PPT} (solid line) corresponds to the transition rate with linear polarization and with LG (0, 1)* spiral-phase mode, respectively.

In Fig. 3 can be noticed that the basic tunnel ADK transition rate has a higher value and that the inclusion of a specific field distribution decreases the transition rate significantly. The obtained result is very interesting; although is not immediately visible, the difference between the values that reach these two transition rates is almost constant. w^{sp}_{ADK},

in the entire laser intensities interval, reaches a value that is in the interval of $86.4976\% - 86.4981\%$ the lower than w_{ADK}.

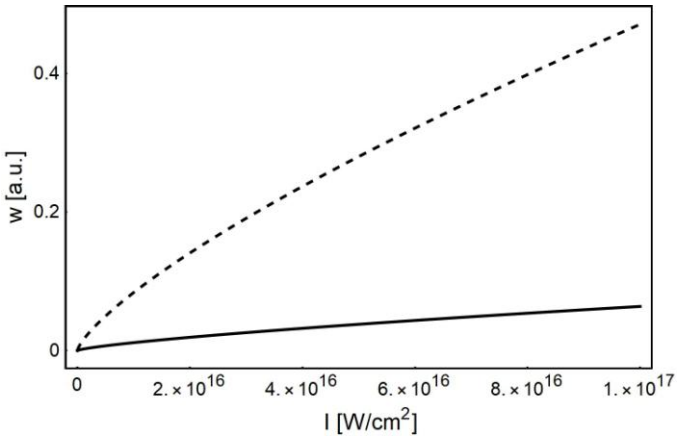

Figure 3. ADK tunneling transition rate as a function of laser intensity. w_{ADK} (dashed line) and w_{ADK}^{sp} (solid line) corresponds to the transition rate with linear polarization and with LG (0, 1)* spiral-phase mode, respectively.

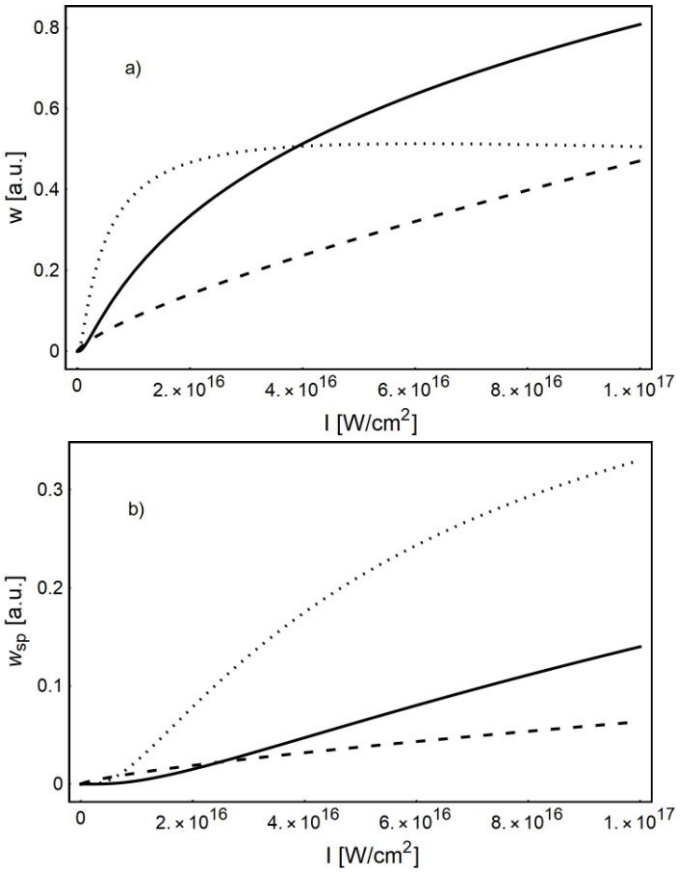

Figure 4. Transition rates as a function of laser intensity; Keldysh theory (solid line), PPT theory (dotted line), ADK theory (dashed line); Pane a) and pane b) corresponds to the transition rate, ω with linear polarization and ω_{sp} with LG (0, 1)* spiral-phase mode, respectively.

We also wanted to show the transition rates given using all three theories on a single graph (Fig. 4). From this figure, it can be seen that, for the same values of the laser intensity, the transition rates given by different theories have various values. We can also notice that the inclusion of LG (0, 1)* spiral-phase field distribution affects transition rates differently. With the inclusion of the specific field distribution $W_{Keldysh}$ and w_{PPT} change, both shapes and values, w_{ADK} retains it's shape, but the values of the transition rates are much smaller.

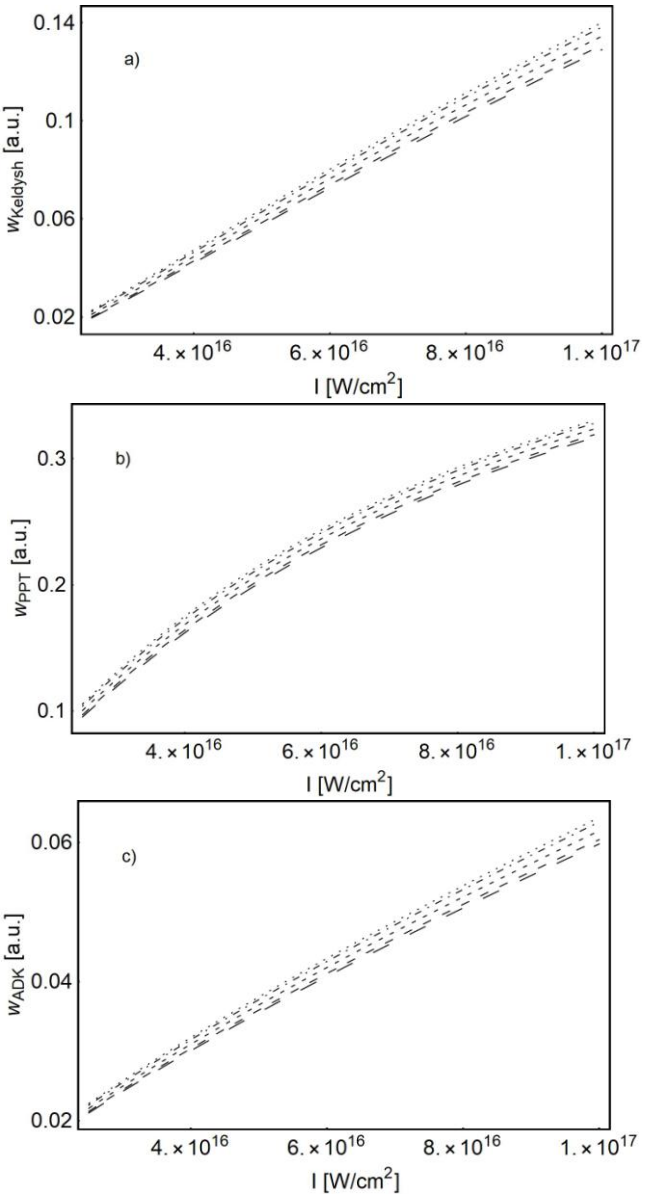

Figure 5. Panes a) $w_{Keldysh}^{sp}$, b) w_{PPT}^{sp} and c) w_{ADK}^{sp} tunneling transition rates as a function of laser intensity for five different azimuthal angles $\phi = -30°$ (dashed large), $\phi = -20°$ (dashed medium), $\phi = 0°$ (dashed small), $\phi = 20°$ (dot-dashed), $\phi = 30°$ (dotted).

At the very end, in order to complete the discussion, we have shown how the transition rates, after LG (0, 1)* spiral-phase field distribution was included, depend on the azimuthal angle (Fig. 5). The azimuthal angle took values $\phi = \{-30°, -20°, 0°, 20°, 30°\}$, while the intensity of the laser field was in the range $I = 10^{14} - 10^{17}\, W/cm^2$. In Fig. 5, it is not possible to see clearly, but for the lower intensities, the changes of the azimuthal angle affect all transition rates. Also, we can observe that in the case of all of three transition rates is the lowest value for $\phi = -30°$, while the highest value is reached for the $\phi = 30°$.

CONCLUSION

The process when an electron leaves an atom by tunneling was analyzed by observing the behavior of the transition rate as a function of laser intensity. We performed our calculation for two physical situations; for basic transition rate with the LG (0, 1)* spiral-phase mode field distribution included. The results show that the Keldysh, PPT and ADK transition rate after inclusion of specific field distributions has a lower value. Also, we must emphasize that this field distribution affects to the different extent within various theories. The greatest decrease is observed for the Keldysh transition rate, and that can be clearly seen in the figure which shows together all the transition rates. It is shown that the value of the transition rate depends on the azimuthal angle. These dependencies are very similar for all three theories. The lowest and highest values transition rates reached for the same angle values.

The analysis clearly establishes the influence of the different laser pulse shapes on all three observed transition rates. Although our result shows a general approach to the tunneling ionization process, it is important for the interpretation and understanding of relevant experimental and theoretical results.

ACKNOWLEDGMENTS

The authors acknowledge funding provided by the University of Kragujevac - Institute for Information Technologies (the contract 451-03-9/2021-14/200378), University of Kragujevac - Faculty of Science (the contract 451-03-9/2021-14/200122) through the grants by the Ministry of Education, Science and Technological Development of the Republic of Serbia.

REFERENCES

Ahmmed, K. M. T., Grambow, C. & Kietzig, A. M. 2014. Fabrication of Micro/Nano Structures on Metals by Femtosecond Laser Micromachining.Micromachines, 5(4), pp. 1219-1253. doi.org/10.3390/mi5041219

Ammosov, V. M., Delone, N. B. & Krainov, V. P. 1986. Tunnel ionization of complex atoms and of atomic ions in an alternating electromagnetic field. Sov. Phys. JETP, 64(6), pp. 1191-1194.

Bauer, D., 2006. Theory of Laser–Matter Interaction, Max--Planck Institute, Heidelberg.

Boutu, W., Auguste, T., Boyko, O., Sola, I., Balcou, Ph., Binazon, L., Gobert, O., Merdji, H., Valentin, C., Constant, E., Mével, E. & Carré, B. 2011. High-order-harmonic generation in gas with a flat-top laser beam, Phys. Rev. A, 84(6), pp. 063406-6. DOI:10.1103/PhysRevA.84.063406

Calvert, J., Xu, H., Palmer, A., Glover, R., Laban, D., Tong, X., Kheifets, A., Bartschat, K., Litvinyuk, I., Kielpinski, D. & Sang, R. 2016. The interaction of excited atoms and few-cycle laser pulses. Sci. Rep., 6(1), 34101-1-34101-9. doi.org/10.1038/srep34101

Ciappina, M. F., Peganov, E. E. & Popruzhenko, S. V. 2020. Focal-shape effects on the efficiency of the tunnel-ionization probe for extreme laser intensities. Matter Radiat. Extremes 5(4), pp. 044401-10. doi.org/10.1063/5.0005380

Corkum, P. B. 1993, Plasma perspective on strong field multiphoton ionization. Phys. Rev. Lett., 71(13), pp.1994–1997. doi.org/10.1103/PhysRevLett.71.1994

Delone, N. B. & Krainov, V. P. 2000. Multiphoton processes in atoms: Springer.

Delone, N. B. & Krainov, V. P. 1999. AC Stark shift of atomic energy levels, Phys. Usp., 42(7), pp. 669–687. https://doi.org/10.1070/PU1999v042n07ABEH000557

Delone, N. B. & Krainov, V. P. 1998. Tunneling and barrier-suppression ionization of atoms and ions in a laser radiation field. Physics Uspekhi, 41(5), pp. 469-485. doi.org/10.1103/PhysRevLett.83.520

Dorn, R., Quabis, S. & Leuchs, G. 2003. Sharper Focus for a Radially Polarized Light Beam. Phys. Rev. Lett., 91(23), pp. 233901. doi.org/10.1103/PhysRevLett.91.233901

Eberly, J. H. & Javanainen, J. 1988. Above-threshold ionization. Eur. J. Phys., 9(4), pp. 265-275. doi.org/10.1088/0143-0807/9/4/004

Eichmann, U., Nubbemeyer, T., Rottke, H. & Sandner W. 2009. Acceleration of neutral atoms in strong short-pulse laser fields. Nature, 461(7268), pp. 1261–1264. doi.org/10.1038/nature08481

Guo, L., Hu, S., Liu, M., Shu, Z., Liu, X., Li, J., Yang, W., Lu, R., Han, S. & Chen, J. 2019. Accuracy of the semiclassical picture of photoionization in intense laser fields (Source: arXiv:1905.00213)

Ho, Phay J. & Eberly, J. H. 2006. In-Plane Theory of Nonsequential Triple Ionization. Phys. Rev. Lett., 97(8), pp. 083001-4. doi: 10.1103/PhysRevLett.97.083001

Ishkhanyan, A M. & Krainov, V P. 2015. Non-exponential tunneling ionization of atoms by an intense laser field. Laser Phys. Lett., 12(4), 046002 (6pp). DOI: 10.1088/1612-2011/12/4/046002

Keldysh, L. V. 1965. Ionization in the Field of a Strong Electromagnetic Wave. Sov. Phys. JETP, 20, pp. 1307-1314.

Krainov, V. P. & Shokri, B. 1995. Energy and angular distributions of electrons resulting from barrier-suppression ionization of atoms by strong low-frequency radiation. JETP, 80(4), pp. 657-661.

Lai, Y. H., Xu, J., Szafruga, U. B., Talbert, B. K., Gong, X., Zhang, K., Fuest, H., Kling, M. F., Blaga, C. I., Agostini, P. & DiMauro, L. F. 2017. Experimental investigation of strong-field-ionization theories for laser fields from visible to midinfrared frequencies, Phys. Rev. A, 96(6), pp. 063417-10. doi.org/10.1103/PhysRevA.96.063417

Landau, L. D. & Lifshitz, E. M. 1991. Course of Theoretical Physics. Vol. 3: Quantum Mechanics: Non Relativistic Theory: Pergamon, Oxford.

Lappas, D. G. & Van Leeuwen, R. 1998. Electron correlation effects in the double ionization of He. J. Phys. B, 31(6), pp. L249-L256. doi:10.1088/0953-4075/31/6/001

Liu, W.-C., Eberly, J. H., Haan, S. L. & Grobe, R. 1999. Correlation Effects in Two-Electron Model Atoms in Intense Laser Fields. Phys. Rev. Lett., 83(3), pp. 520-523.

Machavariani, G., Davidson, N., Lumer, Y. et al., 2007 European Conference on Lasers and Electro-Optics and the International Quantum Electronics Conference, Munich, p. 1.

Machavariani, G., Lumer, Y., .Moshe, I. & Jackel, S. 2007. Effect of the spiral phase element on the radial-polarization (0, 1)* LG beam. Opt. Commun., 271, pp. 190-196. doi:10.1016/j.optcom.2006.10.013

Mainfray, G. & Manus, G. 1991. Multiphoton ionization of atoms. Rep. Prog. Phys., 54(10), pp. 1333-1372. doi.org/10.1088/0034-4885/54/10/002

Ooi, C. H. Raymond, Ho, WaiLoon, & Bandrauk, A. D. 2012. Photoionization spectra by intense linear, circular, and elliptic polarized lasers. Phys. Rev. A, 86(2), pp. 023410-6. DOI:10.1103/PhysRevA.86.023410

Ouyang, J., Perrie, W., Allegre, O. J., Heil, T., Jin, Y., Fearon, E., Eckford, D., Edwardson, S. P. & Dearden G. 2015. Tailored optical vector fields for ultrashort-pulse laser induced complex surface plasmon structuring. Opt. Express, 23(10), pp. 12562-12572. DOI:10.1364/OE.23.012562

Panfili, R., Eberly, J. H. & Haan, S. L. 2001. Comparing classical and quantum dynamics of strong-field double ionization. Opt. Express, 8(7), pp. 431-435. doi.org/10.1364/OE.8.000431

Parker, J. S., Doherty, B. J. S., Taylor, K. T., Schultz, K. D., Blaga, C. I. & DiMauro, L. F. 2006. High-Energy Cutoff in the Spectrum of Strong-Field Nonsequential Double Ionization. Phys. Rev. Lett., 96(13), pp. 133001-4. DOI:10.1103/PhysRevLett.96.133001

Parker, J. S., Smyth, E. S. & Taylor, K. T. 1998. Intense-field multiphoton ionization of helium. J. Phys. B, 31(14), pp. L571-L578. doi.org/10.1088/0953-4075/31/14/001

Perelomov, A. M., Popov, V. S. & Terent'ev, M. V. 1966. Ionization of Atoms in an Alternating Electric Field. Sov. Phys. JETP, 23(5), pp. 924-934.

Schafer, K. J., Yang, B., DiMauro, L. F. & Kulander, K. C. 1993. Above threshold ionization beyond the high harmonic cutoff. Phys. Rev. Lett., 70(11), pp. 1599-1602. doi.org/10.1103/PhysRevLett.70.1599

Shealya, D. L. & Hoffnagle, J. A. 2005. Beam shaping profiles and propagation, Proceedings SPIE Conf. Laser Beam Shaping VI, (San Diego, California, USA), pp. 5876-13. http://people.cas.uab.edu/~dls/publications/spie5876/spie5876-13-electronic.pdf

Shvetsov-Shilovski, N. I., Lein, M. & Tőkési, K. 2019. Semiclassical two-step model for ionization of the hydrogen molecule by strong laser field. Eur. Phys. J. D, 73(2), pp. 1-8. doi.org/10.1140/epjd/e2018-90527-6

Tokarev, V. N., Lopez, J, .Lazare, S. & Weisbuch, F. 2003. High-aspect-ratio microdrilling of polymers with UV laser ablation: experiment with analytical model, Applied Physics A, 76(3), pp. 385-396. doi.org/10.1007/s00339-002-1511-8

Voronov, G. S. & Delone, N. B. 1966. Many-photon ionization of the xenon atom by ruby laser radiation, Sov. Phys. JETP, 23, pp. 54-58.

Xiong, W. & Chin, S. L. 1991. Tunnel ionization of potassium and xenon atoms in a high-intensity CO_2 laser radiation field. Sov. Phys. JETP, 72, pp. 268-271.

Zhang, L. 2010. Intensity spatial profile analysis of a Gaussian laser beam at its waist using an optical fiber system, Chinese Physics Letters, 27(5), pp. 054207-3. DOI:10.1088/0256-307X/27/5/054207

CIP - Каталогизација у публикацији
Народна библиотека Србије, Београд

5

BULLETIN of Natural Sciences Research / editor in chief Branko V. Drljača. - [Štampano izd.]. - Vol. 10, no. 2 (2020)- . - Kosovska Mitrovica : Faculty of Sciences and Mathematics, University of Priština, 2020- (Kruševac : Sigraf). - 29 cm

Polugodišnje. - Je nastavak: The University thought. Publication in natural sciences = ISSN 1450-7226. – Drugo izdanje na drugom medijumu: Bulletin of Natural Sciences Research (Online) = ISSN 2738-1013
ISSN 2738-0971 = Bulletin of Natural Sciences Research (Štampano izd.)
COBISS.SR-ID 28586505

Available Online

This journal is available online. Please visit http://www.bulletinnsr.com to search and download published articles.